

# DIFFERENT MULTIPLE INPUT MULTIPLE OUTPUT SYSTEMS

By  
Mohammed Alamgir  
ID: 3554571

SUBMITTED IN PARTIAL FULFILLMENT OF THE  
REQUIREMENTS FOR THE DEGREE OF  
MASTERS OF ENGINEERING IN ELECTRICAL ENGINEERING  
AT  
VICTORIA UNIVERSITY OF TECHNOLOGY  
MELBOURNE, AUSTRALIA  
MAY 2003

© Copyright by Mohammed Alamgir, 2003

VICTORIA UNIVERSITY OF TECHNOLOGY  
School of Communications and Informatics

The undersigned hereby certify that they have read and recommend to the Faculty of Engineering and Science for acceptance a thesis entitled "**Different Multiple Input Multiple Output Systems**" by **Mohammed Alamgir** in partial fulfillment of the requirements for the degree of **Masters of Engineering in Electrical Engineering**.

Dated: May 2003

Research Supervisor:

\_\_\_\_\_

Prof. Mike Faulkner

Research co-supervisor:

\_\_\_\_\_

Dr. Ying Tan

# VICTORIA UNIVERSITY OF TECHNOLOGY

Date: **May 2003**

Author: **Mohammed Alamgir**

Title: **Different Multiple Input Multiple Output Systems**

Department: **School of Communications and Informatics**

Degree: **M.Eng.** Year: **2004**

Permission is herewith granted to Victoria University of Technology to circulate and to have copied for non-commercial purposes, at its discretion, the above title upon the request of individuals or institutions.

---

Signature of Author

THE AUTHOR RESERVES OTHER PUBLICATION RIGHTS, AND NEITHER THE THESIS NOR EXTENSIVE EXTRACTS FROM IT MAY BE PRINTED OR OTHERWISE REPRODUCED WITHOUT THE AUTHOR'S WRITTEN PERMISSION.

THE AUTHOR ATTESTS THAT PERMISSION HAS BEEN OBTAINED FOR THE USE OF ANY COPYRIGHTED MATERIAL APPEARING IN THIS THESIS (OTHER THAN BRIEF EXCERPTS REQUIRING ONLY PROPER ACKNOWLEDGEMENT IN SCHOLARLY WRITING) AND THAT ALL SUCH USE IS CLEARLY ACKNOWLEDGED.

*To my wife Geeti and our daughter Apona*

# Table of Contents

<b>Table of Contents</b>	<b>v</b>
<b>List of Tables</b>	<b>vii</b>
<b>List of Figures</b>	<b>ix</b>
<b>Abstract</b>	<b>xi</b>
<b>Acknowledgements</b>	<b>xiii</b>
<b>1 Overview of the Thesis</b>	<b>1</b>
<b>2 Introduction</b>	<b>4</b>
2.1 Background . . . . .	5
2.2 Propagation Characteristics of a Radio Channel . . . . .	6
2.2.1 Attenuation . . . . .	6
2.2.2 Multipath Effects . . . . .	7
2.2.3 The Doppler Effect . . . . .	8
2.2.4 Fading . . . . .	8
2.2.5 Fading Distributions . . . . .	9
2.3 Diversity . . . . .	11
2.4 Adaptive Modulation . . . . .	13
2.5 Channel Capacity . . . . .	15
2.5.1 Entropy and Mutual Information . . . . .	15
2.5.2 Channel Capacity . . . . .	16
2.6 Multiple Input Multiple Output Scheme . . . . .	16
2.7 Capacity of MIMO Systems . . . . .	17

2.8	Power Control . . . . .	19
2.9	Outage Capacity . . . . .	21
2.10	Measurement of Capacity . . . . .	22
2.11	Simulation Results . . . . .	23
<b>3</b>	<b>Bell Labs Space Time Architecture</b>	<b>27</b>
3.1	Introduction . . . . .	28
3.2	Detection Process . . . . .	29
3.2.1	Nulling . . . . .	29
3.2.2	Interference Cancellation . . . . .	30
3.3	Optimal Detection Order . . . . .	31
3.4	Computing the ZF Nulling Vector . . . . .	31
3.5	Computing the MMSE Nulling Vector . . . . .	32
3.6	Detection Algorithm . . . . .	32
3.7	Complexity Analysis . . . . .	33
3.8	QR Decomposition Based Detection . . . . .	35
3.9	Backward and Forward Sweeps . . . . .	37
3.10	Optimal Ordering . . . . .	38
3.11	Complexity Analysis of the QR Decoder . . . . .	39
3.12	Simulation Results . . . . .	39
3.12.1	BER, BLER and Throughput . . . . .	40
3.12.2	Execution Time . . . . .	45
<b>4</b>	<b>New Detection Method for VBLAST</b>	<b>47</b>
4.1	The Polar Decomposition . . . . .	48
4.2	Detection Using the Cholesky Factorization . . . . .	48
4.3	Detection Using the QR Factorization . . . . .	49
4.4	Optimal Ordering . . . . .	50
4.5	Properties of the Polar Decomposition . . . . .	50
4.6	Behavior of Q and P Matrices . . . . .	51
4.7	Algorithms for the Polar Decomposition . . . . .	51
4.7.1	Higham's Algorithm for Polar Decomposition . . . . .	52
4.8	Complexity Analysis . . . . .	54

4.9	Simulation Results . . . . .	54
4.9.1	BER, BLER and Throughput . . . . .	54
4.9.2	Execution Time . . . . .	55
<b>5</b>	<b>Singular Value Decomposition Based MIMO Systems</b>	<b>58</b>
5.1	Introduction . . . . .	59
5.2	SVD Based MIMO Systems . . . . .	59
5.3	Behavior of U, D and V Matrices . . . . .	61
5.4	SNR of Parallel Subchannels . . . . .	62
5.5	Power Control . . . . .	63
5.6	Adaptive Modulation across Subchannels . . . . .	64
5.7	Simulation Results . . . . .	64
<b>6</b>	<b>Performance Comparison Results</b>	<b>67</b>
6.1	Introduction . . . . .	67
6.2	Channel Models . . . . .	68
6.2.1	IID Channels . . . . .	68
6.2.2	Slow Fading Rayleigh Channel . . . . .	69
6.2.3	VUT Measured Channel . . . . .	69
6.3	Variants of VBLAST . . . . .	69
6.3.1	BER, BLER and Throughputs . . . . .	70
6.3.2	Execution Time . . . . .	72
6.4	VBLAST System vs SVD-based System . . . . .	73
6.4.1	IID Channels . . . . .	75
6.4.2	IID Rank Deficient Channel . . . . .	78
6.4.3	Slow Fading Rayleigh Channel . . . . .	79
6.4.4	VUT Measured Channel . . . . .	80
<b>7</b>	<b>Conclusion and Further Work</b>	<b>86</b>
	<b>Bibliography</b>	<b>88</b>

# List of Tables

6.1	Acronyms used to denote different MIMO systems. . . . .	68
6.2	Complexities of different VBLAST methods. . . . .	72
6.3	Correlation among the singular values of measured channels. . . . .	83

# List of Figures

2.1	Typical Rayleigh fading of a signal. . . . .	10
2.2	PDFs of Rayleigh and Ricean distributions. . . . .	11
2.3	$E_S/N_0$ vs BER for MQAM constellations. . . . .	14
2.4	MIMO transmission scheme. . . . .	17
2.5	Mean capacity of different MIMO systems. . . . .	24
2.6	Capacity CCDFs of different MIMO systems at SNR = 0dB. . . . .	24
2.7	MIMO capacity CCDF for different SNRs. . . . .	25
2.8	MIMO mean capacity with waterfilling, ( $4 \times 4$ system). . . . .	26
3.1	The VBLAST architecture. . . . .	29
3.2	Bit error rate of the VBLAST system in IID random channel. . . . .	40
3.3	Block error rate of the VBLAST system in IID random channel. . . . .	41
3.4	Throughput of the VBLAST system in IID random channel. . . . .	41
3.5	Bit error rate of the VBLAST system in IID random channel with optimal ordering. . . . .	42
3.6	Bit error rate of QR based VBLAST system in IID random channel. . . . .	43
3.7	Effect of optimal ordering on bit error rate. . . . .	43
3.8	Effect of optimal ordering and backward/forward sweep on bit error rate. . . . .	44
3.9	Throughput of QR-based VBLAST system. . . . .	44
3.10	Theoretical complexity of the VBLAST and QR methods. . . . .	46
3.11	Execution time of the VBLAST and QR methods. . . . .	46
4.1	Polar Decomposition behavior . . . . .	52
4.2	Bit error rate of Polar Decomposition-based VBLAST. . . . .	55
4.3	Block error rate of Polar Decomposition-based VBLAST. . . . .	56
4.4	Throughput of Polar Decomposition-based VBLAST. . . . .	56
4.5	Complexity of VBLAST and Polar Decomposition-based VBLAST. . . . .	57

4.6	Execution time of VBLAST and Polar Decomposition-based VBLAST. . .	57
5.1	SVD-based MIMO transmission scheme. . . . .	60
5.2	SVD-based MIMO transmission in TDD channel (taken from [22]). . .	61
5.3	Changes in U, V and D matrices for a slowly varying channel matrix H.	62
5.4	Bit error rate of the SVD system. . . . .	65
5.5	Throughput of the SVD system. . . . .	66
6.1	Floor map of the measurement. Rx is receiver position, A is LOS point and B is NLOS point. . . . .	70
6.2	Bit error rate of VBLAST for different decoding methods. . . . .	71
6.3	Bit error rate of different VBLAST decoding methods with optimal decoding order. . . . .	72
6.4	Theoretical complexity of VBLAST decoding methods. . . . .	74
6.5	Execution time of VBLAST decoding methods. . . . .	74
6.6	CPU time of VBLAST decoding methods. . . . .	75
6.7	Throughput of different MIMO systems. . . . .	76
6.8	Block error rate of different MIMO systems. . . . .	77
6.9	Bit error rate of different MIMO systems. . . . .	77
6.10	Effect of the optimal order and waterfilling. . . . .	78
6.11	Throughputs of VBLAST-ZF-opt and SVD-adap systems in rank defi- cient IID channel. . . . .	79
6.12	Bit error rate of VBLAST-ZF-opt and SVD-adapt systems in rank de- ficient IID channel . . . . .	80
6.13	Throughput of VBLAST-opt system in slow fading Rayleigh channel. . .	81
6.14	Throughput of SVD-adapt system in slow fading Rayleigh channel. . .	81
6.15	Singular values of measured channel with LOS path. . . . .	82
6.16	Singular values of measured channel with NLOS path. . . . .	82
6.17	Throughputs of VBLAST-ZF-opt and SVD-adapt systems in measured channel. . . . .	84
6.18	Bit error rates of VBLAST-ZF-opt and SVD-adapt systems in measured channel. . . . .	84

# Abstract

The use of multiple antennas at the transmitter as well as at the receiver can greatly improve the capacity of a wireless link when operating in a rich scattering environment. In such an arrangement all transmitting antennas radiate in the same frequency band so the overall spectral efficiency becomes very high. Such a multiple antenna scheme, popularly known as Multiple Input Multiple Output (MIMO) has potential application in wireless local area networks (WLAN) and cellular micro-cells. One reason is that the WLANs and other short range wireless systems often operate in an indoor environment, which offers rich scattering. The other reason is the demand for higher data rates in cellular and WLAN systems to cater for multimedia services. Recently researchers have proposed different architectures for materializing the potential of the MIMO scheme. VBLAST (Vertical-Bell Labs Space Time) is a popular architecture that will play an important role in future standardizations. Furthermore, different decoding methods have been proposed for VBLAST. The SVD (Singular Value Decomposition) based system is envisioned as a highly effective MIMO technique in a TDD (Time Division Duplex) framework. Such a system operates by adapting the constellation size across different subchannels.

In this work we study the VBLAST and SVD architectures and compare the performance and computing power requirement of these architectures. Also in this study a new efficient decoding method for the VBLAST architecture is proposed. The original VBLAST decoding method relies on the repetitive computation of the pseudoinverse

of the channel matrix. Alternatively, there are methods based on the QR decomposition, the matrix square root etc. Our new decoding method is based on a relatively less known matrix decomposition, the Polar Decomposition. The new method requires less computation and has several other advantages like the possibility of incremental updates, channel rank tracking, etc. We consider three different types of channels: IID random, slow fading and measured channels. The entire work is simulated in the MATLAB environment.

The main contribution of this work includes: a comparative study and a head to head comparison of the VBLAST and SVD-based MIMO systems. The application of adaptive modulation in the SVD-based system and the introduction of a new efficient decoding method for the VBLAST system are also included. Simulation results are reported with comments and conclusions.

# Acknowledgements

I would like to thank my supervisor Professor Mike Faulkner, who first has rescued me from the frustration of doing course work and then continued his support and direction during the course of this research. Without his generous help it would have been impossible to finish this work.

Next comes cosupervisor Ying Tan who has offered his maximum help to get me into MIMO and kept his support continuous. Also thanks for Melvyn Pierra, Guillame Lebrun and Jason Gao at Telecommunication and Microelectronics Center. They have helped me by providing papers, suggestions and in many other ways.

The AusAID has provided the funds for my study and living through a scholarship. AusAID liaison officer, Kerry Wright was my resort in bad times in Melbourne; she deserves special mention.

A heartfelt gratitude for the people of Bangladesh who have supported my undergraduate study in Bangladesh. Also thanks to Shahjalal University of Science and Technology, Sylhet, Bangladesh for approving me of Study Leave to pursue this degree.

I am grateful to my parents for bringing me into this world and to my siblings for keeping a warm family where I grew up. My wife Geeti has always supported me and deserves more than mere acknowledgement.

Finally, I wish to thank Gavin, Trung, Andrew, Edward and Way Wu for spending a wonderful time in the room D708. The Thursday soccer team is also owed thanks.

**Mohammed Alamgir**

Melbourne, Australia

# Chapter 1

## Overview of the Thesis

This chapter gives an overview of the contents of this thesis. The chapters of interest are the following:

- **Chapter 1 Overview of the thesis**
- **Chapter 2 Introduction:** Chapter two starts by discussing the characteristics of the radio channel such as attenuation, multipath, the Doppler effect and fading. Transmit diversity techniques are introduced and different techniques are discussed briefly. A short paragraph shows how adaptive modulation techniques can counter fading. Information theoretic terms such as entropy, mutual information and capacity are elaborated. An introduction to the MIMO scheme is given followed by the calculation of the theoretical capacity. Power control issues are discussed. The definitions of outage capacity and system throughput, the practical ways of measuring capacity, are given. Some simulation results are then shown. Most of the concepts presented in this chapter are known.
- **Chapter 3 Bell Labs Space Time Architecture:** This chapter deals with

the aspects of the VBLAST architecture. An introduction to the VBLAST architecture is given followed by its operation. The detection method, nulling, interference cancellation, and optimal ordering are discussed thoroughly. The decoding algorithm is studied, and an exact unreported complexity analysis of the decoding algorithm is done. Then it is shown how the QR decomposition can be used to decode VBLAST signals. Benefits of forward and backward sweeps are considered, including ordering for optimal detection. A calculation of complexity follows. The chapter ends with some simulation results showing the performances of the original VBLAST and the QR method.

- **Chapter 4 New Detection Method for VBLAST:** One of the two major contributions of the present work and this thesis is in this chapter. The chapter introduces a new detection method for the VBLAST system using a relatively less known matrix decomposition, the Polar Decomposition (PD). The Polar Decomposition is introduced and Cholesky and QR factorizations are used to decode the VBLAST signals. The issue of optimal ordering is also discussed. The properties of the PD are discussed, and then it is shown how these properties are conducive to the VBLAST detection. Algorithms for the PD are reviewed with complexity analysis. The chapter ends with some simulation results and comments.
- **Chapter 5 Singular Value Decomposition Based MIMO Systems:** This

chapter introduces the Singular Value Decomposition (SVD)-based MIMO system. Such systems are suitable for Time Division Duplex (TDD) mode of communication and can get very close to the theoretical capacity limit. The detailed architecture and properties of the SVD system are discussed. The SVD produces parallel subchannels of different gains and adaptive modulation is used across them. Power control issues are also addressed. The chapter concludes with some simulation results and comments.

- **Chapter 6 Performance Comparison Results:** This chapter contains the results of the simulations performed under different conditions. Three types of channel models are considered. They are: the IID (independently and identically distributed) random channel, a slow fading Rayleigh channel and a physical channel measured by the VUT MIMO group. The BER performance and execution time of the different decoding methods for VBLAST are reported. A comparison between VBLAST and SVD systems is also performed.
- **Chapter 7 Conclusion and Further Work:** The main observations of the thesis are remarked in this chapter. This chapter ends by hinting at the scope and possible directions for further work.

# Chapter 2

## Introduction

### Chapter Outline

This chapter starts by discussing the characteristics of radio channels such as attenuation, multipath, the Doppler effect and fading (section 2.2). Transmit diversity techniques are introduced in section 2.3, and then section 2.4 shows how adaptive modulation techniques can counter the fading. Information theoretic terms such as entropy, mutual information and capacity are elaborated in section 2.5. Section 2.6 introduces the MIMO scheme followed by a calculation of the theoretical capacity of the MIMO channel. The definitions of outage capacity and system throughput, the practical ways of measuring capacity, are given in sections 2.9 and 2.10 respectively. Some simulation results are then shown in section 2.11. The chapter ends making a few comments. Most of the concepts presented in this chapter are classical.

## 2.1 Background

Wireless devices such as mobile phones have been gaining more and more popularity mainly because of their mobility. Though voice was the only service available on early phones, text service has now been added, and more recently multimedia services, such as pictures and videos have started to emerge. These services are not widespread, but the demand for them is on the rise. At the same time wireless local area networks (WLAN) still have to compete with their wireline counterparts mainly because of their high data rates. Wireless local area networks are attractive for their mobility, but the high data rates available on the wireline network still seem to be unreachable in wireless networks. A requirement for high data rates directly translates into a wider bandwidth requirement which is not feasible because of the limited radio spectrum. Nevertheless, digital wireless systems are slowly replacing ordinary analog ones. Examples include the new standards for radio and television broadcast, the digital audio broadcasting, DAB and digital video broadcasting, DVB.

The increasing adoption of multimedia and demand for mobility in computer networks have resulted in a huge wireless research effort in recent years. Given the limited radio spectrum and unfriendly propagation conditions, designing reliable high data rate wireless networks has a lot of problems. The maximum capacity of a radio channel with a given bandwidth is limited by the well known Shannon [1] formula. The Shannon limit gives the maximum limit on capacity but does not say anything about how to achieve that limit. Various techniques have been proposed to counter the problem of propagation conditions, and achieved data rates are now very close to

the Shannon limit. Data transmission at rates higher than the Shannon limit have never been thought possible until very recently.

## 2.2 Propagation Characteristics of a Radio Channel

In a real environment radio waves from mobile devices travel through the air, buildings and other obstacles. Reflections from different objects cause the waves to travel through multiple paths to the receiver. The movement of objects in the channel or that of the receiver cause an apparent shift in the carrier frequency. A reliable communication system tries to overcome or take advantage of these channel perturbations.

### 2.2.1 Attenuation

Attenuation is the loss of average received signal power. Factors responsible for attenuation are the distance between the transmitter and receiver, the obstacles in between, their physical properties, etc. Attenuation due to distance increases exponentially, and, in addition to this, the presence of very large obstacles such as buildings, hills, etc causes another type of attenuation known as log normal shadowing. Geometric models have been proposed to explain these large scale power losses but statistical models are often used because of their accurate description of particular real environments. Statistically, the attenuation is considered as a random variable having a well known distribution. A common formula used to model attenuation is

$$PL(d)[dB] = \overline{PL}(d_0) + 10n \log \left( \frac{d}{d_0} \right) + X_\sigma \quad (2.2.1)$$

where,  $X_\sigma$  is a zero mean Gaussian distributed random variable (in dB) with standard deviation  $\sigma$  (also in dB) and accounts for the log normal shadowing effect. The path loss at any arbitrary distance  $d$  is statistically described relative to the close-in reference point  $d_0$ , the path loss exponent  $n$ , and the standard deviation  $\sigma$ . The exponent  $n$  can have values from 1.6 (in indoor line of sight) up to 6 (in highly builtup cities).

### 2.2.2 Multipath Effects

Radio waves traveling along different paths arrive at the receiver at different times with random phases and combine constructively or destructively. The net result is a rapid fluctuation in the amplitude of the received signal in a short period of time or distance travelled. However, the large scale average path loss remains constant. Multipath propagation had previously been considered a problem, but now it is exploited to achieve higher capacity.

The multipath structure of a channel is quantified by its *delay spread* or by its root-mean-square (RMS) value. A channel having delay spread less than the symbol period of transmission offers frequency nonselective attenuation, and a larger value of delay spread means there is frequency selective variation in the channel. Another parameter, the *coherence bandwidth* is also often used to describe the frequency selectiveness and is related to the delay spread as

$$B_c \approx \frac{1}{50\sigma_\tau} \quad (2.2.2)$$

where,  $\sigma_\tau$  is the RMS delay spread [23].

### 2.2.3 The Doppler Effect

When there is relative movement between the transmitter and receiver, the carrier frequency, as perceived by the receiver, gets changed by some amount; this is known as the Doppler effect. The amount of frequency shift depends on the relative speed, the direction of movement and the frequency of the carrier. In mathematical terms

$$f_d = \frac{v}{\lambda} \times \cos \theta \quad (2.2.3)$$

where  $v$  is the relative speed between the transmitter and receiver,  $\theta$  is the angle between the direction of motion and the wave propagation, and  $\lambda$  is the carrier wavelength. A Doppler shift can be negative as well as positive, meaning an apparent decrease or increase in frequency, respectively. However, most often the maximum absolute value is considered and normalized with respect to the symbol rate and denoted by  $F_d T$

$$F_d T = \frac{|f_d|}{f_{symbol}} \quad (2.2.4)$$

where  $f_{symbol}$  is the symbol rate. A typical office environment has  $F_d T$  value of about  $2^{-3}$ . Another parameter, often used to characterize the time varying nature of the channels is the *coherence time* which is related to the Doppler shift by

$$T_c \approx \frac{9}{16\pi f_m} \quad (2.2.5)$$

where  $f_m$  is the maximum Doppler shift given by  $f_m = v/\lambda$  [23].

### 2.2.4 Fading

The result of multipath and the Doppler shift is fading. Fading is the rapid variation in signal strength over a short distance or time interval where the large scale attenuation

is constant. A fade can be flat or frequency selective depending on the multipath structure of the channel, and slow or fast depending on the Doppler effect. Flat fading occurs when the bandwidth of the signal is less than the coherence bandwidth. This type of fading is common, and some communication systems are designed specifically to operate in very narrow bandwidth mode. If the signal bandwidth is wider than the coherence bandwidth then different frequencies undergo independent fading and the result is *inter-symbol-interference* (ISI).

How rapidly the channel changes as compared to the signal variation determines whether the fading is slow or fast. The Doppler effect is the reason for this type of fading as any movement of the receiver or any object in the channel produces a Doppler shift. The symbol period of the transmitted signal has to be shorter than the coherence time for a slow fading channel.

A channel can be either flat or frequency selective and either slow or fast fading. A typical office environment is slow fading. New techniques (such as OFDM) are designed to use very low bandwidth subchannels so that the fading can be regarded flat. Fig. 2.1 shows typical fading for a signal with an  $F_d T$  value of 0.02.

### **2.2.5 Fading Distributions**

The fading effect is usually described statistically using the Rayleigh distribution. The amplitude of two quadrature Gaussian signals follows the Rayleigh distribution whereas the phase follows a uniform distribution. The probability distribution function (PDF)

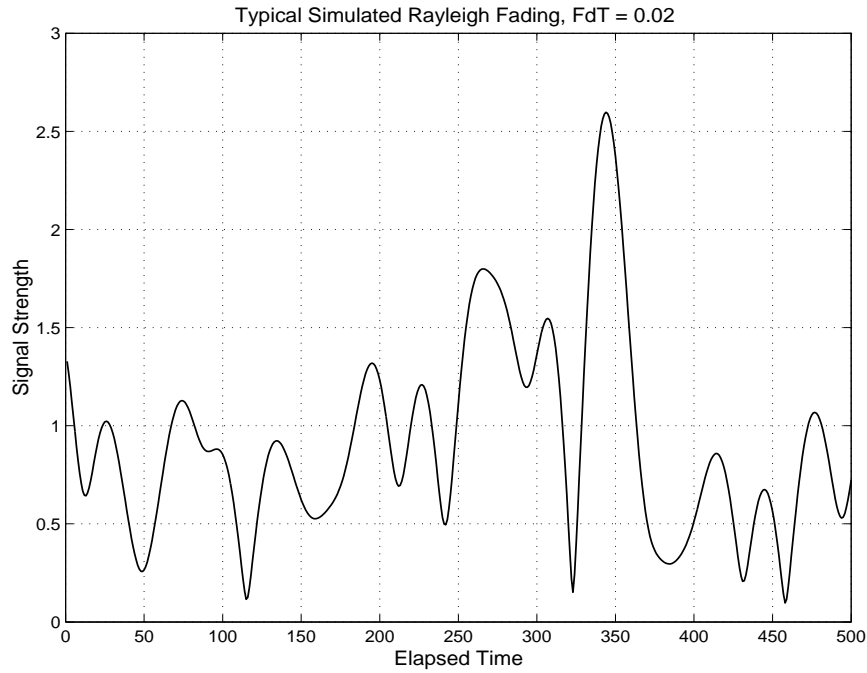


Figure 2.1: Typical Rayleigh fading of a signal.

of a Rayleigh distribution is given by

$$p(r) = \begin{cases} \frac{r}{\sigma^2} \exp\left(-\frac{r^2}{2\sigma^2}\right) & (0 \leq r < \infty) \\ 0 & (r < 0) \end{cases} \quad (2.2.6)$$

where  $\sigma$  is the RMS (amplitude) value of the received signal and  $\sigma^2$  is the average power. In an indoor environment where the chance of a line of sight path is high, the fading follows a Ricean distribution with PDF

$$p(r) = \begin{cases} \frac{r}{\sigma^2} \exp\left(-\frac{r^2+A^2}{2\sigma^2}\right) I_0\left(\frac{Ar}{\sigma^2}\right) & (A \geq 0, r \geq 0) \\ 0 & (r < 0) \end{cases} \quad (2.2.7)$$

where  $A$  is the peak amplitude of the dominant path and  $I_0(\cdot)$  is the modified Bessel function of the first kind and order zero. Fig. 2.2 shows the PDFs of Rayleigh and Ricean distributions.

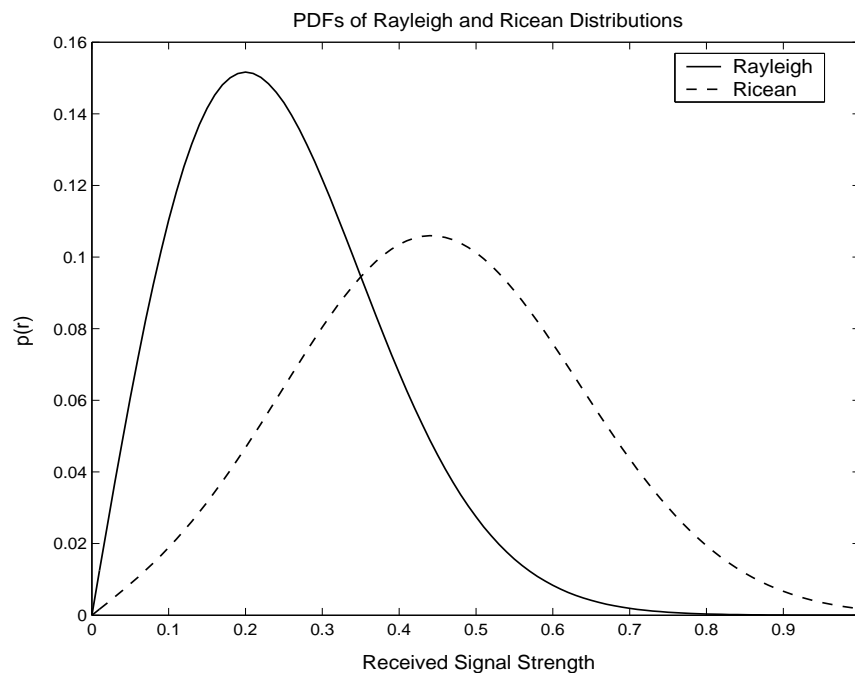


Figure 2.2: PDFs of Rayleigh and Ricean distributions.

## 2.3 Diversity

In a scattering environment the individual signal path arriving at the receiver faces independent or highly uncorrelated fading. This means that when a particular signal path is in a fade there may be another signal path not in any fade. The receiver can exploit this fact by receiving more than one path and choosing and/or combining them. Widely used schemes to do this are: selection diversity where the path with the best average signal to noise ratio (SNR) is chosen, equal gain combining where the different paths are cophased and added together and MMSE combining where the different paths are weighted and then added (weighting coefficients are chosen during a training phase). Receiver diversity can improve the average SNR by 20dB to 30dB.

In practice, diversity techniques can be applied in the space, polarization, frequency or time domains.

- **Space Diversity:** Also known as antenna diversity, space diversity uses more than one antenna at the receiver. The signals received on antennas separated by a half wavelength or more tend to be decorrelated [2]. This is because in a rich scattering environment the chance of a line of sight path is low, and most paths are reflected or diffracted from obstacles. Usually antenna diversity is used only at the base station because multiple antennas on the portable unit pose a design challenge and do not justify the cost.
- **Polarization Diversity:** Electromagnetic waves have vertical and horizontal polarizations that also show decorrelation [3]. Where the required antenna spacing for space diversity is not feasible, polarization diversity is used as an alternative as the same antenna can be used for different polarizations. However, it is not possible to have more than 2-way polarization diversity.
- **Frequency Diversity:** Frequencies separated by more than the coherence bandwidth of the channel suffer independent fades. Frequency diversity takes advantage of this fact by transmitting at more than one carrier frequency. The GSM standard uses frequency hopping to achieve frequency diversity.
- **Time Diversity:** In time diversity the same information symbol is repeatedly transmitted at different time slots with the hope that they will suffer independent fading and the receiver will combine them properly. While highly effective in fast fading environments, time diversity is not as effective in slow fading channels unless a large decoding delay can be tolerated. A coding structure known as *interleaving* is often used to realize time diversity where the receiver knows the

code before any transmission takes place.

## 2.4 Adaptive Modulation

Traditional communication systems use fixed constellations among which QPSK and MQAM are popular. A QPSK constellation uses two quadrature carriers each of which is BPSK modulated. In MQAM the phase as well as the amplitudes of a pair of quadrature carriers are varied according to the binary data. Whereas QPSK can transmit a maximum two bits per symbol, MQAM can send  $\log_2 M$  bits per symbol. However, higher level constellations have higher probabilities of error thus requiring higher SNRs to achieve a given bit error rate (BER). The symbol error rate (SER) of an MQAM constellation with ideal detection is bounded by [4]

$$P_S \leq 1 - \left[ 1 - 2Q \left( \sqrt{\frac{3E_S}{(M-1)/N_0}} \right) \right]^2 \quad (2.4.1)$$

where  $E_S$  is the average symbol energy,  $N_0$  is the Gaussian noise power,  $M$  is the constellation size and  $Q(\cdot)$  is the Q-function. The BER is related to the SER by

$$P_B = \frac{2^{k-1}}{2^k - 1} P_S \quad (2.4.2)$$

where  $k = \log_2 M$ . A plot of BER vs  $E_s/N_0$  for different  $M$  is shown in Fig. 2.3.

In a fading channel, the received signal power varies over time. One way to compensate for this effect is by adapting the constellation size based on fading statistics. This ensures overall fewer bit errors. However, there has to be some form of feedback to the transmitter about the fading conditions, and the receiver must know which particular constellation is being used by the transmitter. In a Time Division Duplex

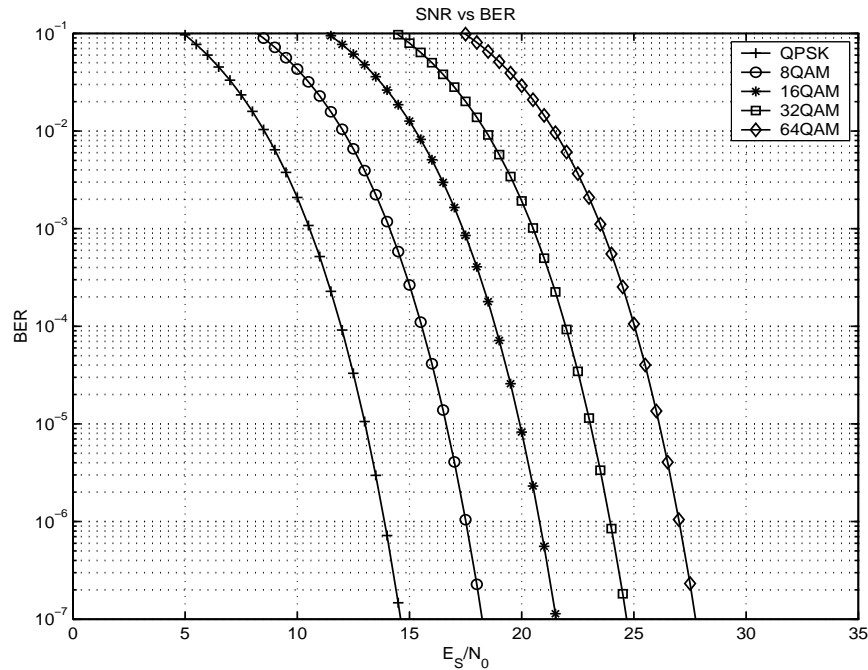


Figure 2.3:  $E_S/N_0$  vs BER for MQAM constellations.

(TDD) scheme both ends of the communication link have knowledge of the channel, and so they can adapt the constellation size without extra feedback. To make a decision about the size of the constellation, the average available SNR (which signifies the channel condition) and maximum acceptable target BER should be given. In some applications (such as speech) the overall throughput is important and bit errors are not critical, while in other applications (like file transfers) a very low BER is more important than the throughput.

In an ideal situation, a continuous adaptation of the constellation is required but in practice one can have only integer constellation sizes. Constellation sizes of  $2^k$  i.e, 2, 4, 8, 16, 32, etc are used commonly. In [5] it was shown that even such a discrete adaptation can closely approximate the ideal case. In this work we use only square constellations such as QPSK, 16QAM and 64QAM. Also  $10^{-6}$  is the maximum

acceptable BER and hence lower bounds the minimum SNR required for each of these constellations. Fig. 2.3 implies that if the available SNR is 27dB or more 64QAM should be used; if the SNR degrades to between 21dB and 24dB, 16QAM should be used. If the SNR is between 13dB and 17.5dB QPSK should be used. At an SNR less than 13dB transmission would stop.

## 2.5 Channel Capacity

### 2.5.1 Entropy and Mutual Information

The *entropy* of a discrete random variable  $X$  is defined as [6]

$$\mathcal{H}(X) = - \sum_{j=1}^n p_j \log_2(p_j) \quad (2.5.1)$$

where  $p_j$  is the probability that  $X = j$ . Entropy measures the uncertainty of a random variable, and so, it is an indication of the information contained in that variable [6].

Based on the joint probability, the *joint entropy* of two random variables  $X, Y$  is defined to be

$$\mathcal{H}(X, Y) = - \sum_{j=1}^n \sum_{k=1}^m p_{jk} \log_2(p_{jk}) \quad (2.5.2)$$

where  $p_{jk}$  is the joint probability that  $X = j$  and  $Y = k$ . If  $X$  and  $Y$  are dependent and  $p_j(k)$  denotes the conditional probability that  $Y = k$  given  $X = j$ , then the *conditional entropy* of  $Y$  given  $X$ , denoted by  $\mathcal{H}(Y|X)$  is defined as

$$\mathcal{H}(Y|X) = - \sum_{j=1}^n \sum_{k=1}^m p_{jk} \log_2(p_j(k)) \quad (2.5.3)$$

The *mutual information* of two random variables,  $X$  and  $Y$ , denoted as  $\mathcal{I}(X; Y)$  is given by

$$\mathcal{I}(X; Y) = \mathcal{H}(Y) - \mathcal{H}(Y|X) \quad (2.5.4)$$

For any two random variables  $X$  and  $Y$ ,  $\mathcal{I}(X;Y) = \mathcal{I}(Y;X)$ . Also  $\mathcal{I}(X;Y) = 0$  when  $X$  and  $Y$  are independent.

### 2.5.2 Channel Capacity

Shannon [1] defines the capacity of a channel as the maximum data rate at which data transmitted from a transmitter, when passed through the channel, can be *received* at some receiver with negligible chance of error. If the data source and received data are viewed as random variables, then the channel capacity refers to the maximum mutual information between them. The capacity  $C$  is

$$C = \max_{p(x)} \mathcal{I}(X;Y) \quad (2.5.5)$$

where the maximization is taken over all possible probability distributions  $p(x)$  of  $X$ . A data source with Gaussian probability distribution has the maximum entropy. Thus, to achieve a data rate close to the capacity, the data source should be Gaussian distributed. For a bandlimited channel with noise being Gaussian and white, Shannon [1] derived the normalized capacity (capacity per unit bandwidth) to be

$$C = \log_2(1 + \rho) \text{ bps/Hz} \quad (2.5.6)$$

where  $\rho$  is the received SNR.

## 2.6 Multiple Input Multiple Output Scheme

The multiple input multiple output (MIMO) scheme deploys multiple antennas at the receiver as well as at the transmitter. The data stream from a single user is demultiplexed and fed into the transmitting antennas all of which radiate in the same frequency

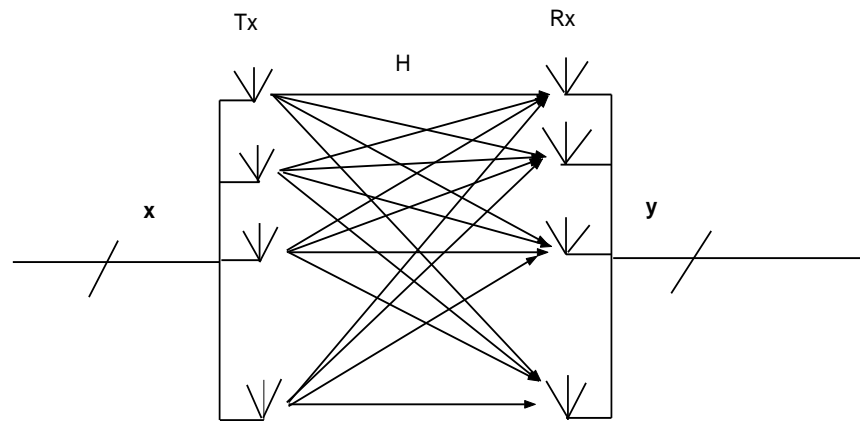


Figure 2.4: MIMO transmission scheme.

band. By sharing the same frequency band the spectral efficiency becomes very high. The receiver is assumed to have ideal channel estimates so it can separate and decode the symbols transmitted from each antenna. The ability to separate out the symbols is due to the fact that in a scattering environment, the signals received at each receiving antenna from each transmitting antenna appear to be uncorrelated. Fig.2.4 shows a block diagram of such a scheme.

## 2.7 Capacity of MIMO Systems

A baseband MIMO system with  $t$  transmit antennas and  $r$  receive antennas can be modelled by the linear relationship

$$\mathbf{y} = H\mathbf{x} + \mathbf{n} \quad (2.7.1)$$

where  $\mathbf{x}$  is the  $(t \times 1)$  transmit vector,  $\mathbf{y}$  is the  $(r \times 1)$  receive vector,  $H$  is the  $(r \times t)$  channel matrix and  $\mathbf{n}$  is the  $(r \times 1)$  additive white Gaussian noise vector. The channel is assumed to be flat (narrow bandwidth) and slow fading so it does not change during a burst of transmission. Each entry of  $H$ ,  $h_{ij}$  represents the complex path gain

between the  $j$ th transmit antenna and  $i$ th receive antenna. With  $h_{ij}$  being complex Gaussian, the magnitude  $|h_{ij}|$  is Rayleigh distributed. In a rich scattering environment the columns of  $H$  are assumed to be independent.

The mutual information is then

$$\begin{aligned}
 \mathcal{I}(\mathbf{x}; \mathbf{y}) &= \mathcal{H}(\mathbf{y}) - \mathcal{H}(\mathbf{y}|\mathbf{x}) \\
 &= \mathcal{H}(\mathbf{y}) - \mathcal{H}((H\mathbf{x} + \mathbf{n})|\mathbf{x}) \\
 &= \mathcal{H}(\mathbf{y}) - \mathcal{H}(\mathbf{n}|\mathbf{x}) \\
 &= \mathcal{H}(\mathbf{y}) - \mathcal{H}(\mathbf{n})
 \end{aligned} \tag{2.7.2}$$

where the transmit vector  $\mathbf{x}$  and noise vector  $\mathbf{n}$  are assumed independent of each other.

The third equality holds because  $H$  is constant (zero entropy) during the transmission of a whole block of  $\mathbf{x}$ . Eq. (2.7.2) is maximized when  $\mathbf{y}$  has the maximum entropy of  $\log_2 \det(\pi e K)$ . This requires  $\mathbf{y}$  to be a circularly symmetric complex Gaussian vector with covariance matrix  $E\{\mathbf{y}\mathbf{y}'\} = K$  [7] where  $'$  denotes complex conjugate transpose. If the transmit vector  $\mathbf{x}$  is also complex Gaussian vector with covariance  $E\{\mathbf{x}\mathbf{x}'\} = Q$ , then  $K$  can be found by

$$\begin{aligned}
 K &= E\{(H\mathbf{x} + \mathbf{n})(H\mathbf{x} + \mathbf{n})'\} \\
 &= E\{H\mathbf{x}\mathbf{x}'H'\} + E\{\mathbf{n}\mathbf{n}'\} \\
 &= HQH' + K^n \\
 &= K^s + K^n
 \end{aligned} \tag{2.7.3}$$

where the fact that  $\mathbf{x}$  and  $\mathbf{n}$  are independent and zero mean is used. Here  $K^s$  and  $K^n$  are respectively the signal and noise parts of the observation covariance matrix. The

maximum mutual information, which is also the capacity, is

$$\begin{aligned}
C &= \mathcal{H}(\mathbf{y}) - \mathcal{H}(\mathbf{n}) \\
&= \log_2 [\det (\pi e (K^s + K^n))] - \log_2 [\det (\pi e K^n)] \\
&= \log_2 [\det ((K^s + K^n) (K^n)^{-1})] \\
&= \log_2 [\det (K^s (K^n)^{-1} + I_r)] \\
&= \log_2 [\det (HQH' (K^n)^{-1} + I_r)] \tag{2.7.4}
\end{aligned}$$

where  $I_r$  is the  $r \times r$  identity matrix. The noise received at each receiving antenna is assumed to be uncorrelated so,  $K^n = \sigma^2 I_r$ ,  $\sigma^2$  being the noise power on each receiving antenna. Also, when the transmitter has no knowledge about the channel, it is optimum to use equal power on each antenna [7]; that means  $Q = \frac{P_t}{t} I_t$ ,  $P_t$  being the total signal power. The MIMO channel capacity then becomes

$$C = \log_2 \left[ \det \left( I_r + \frac{\rho}{t} HH' \right) \right] \tag{2.7.5}$$

where  $P_t/\sigma^2$  has been replaced by  $\rho$ , the average SNR at each receiving antenna.

## 2.8 Power Control

According to the singular value theorem [16], any matrix  $H \in \mathbb{C}^{r \times t}$  can be decomposed as

$$H = UDV' \tag{2.8.1}$$

where  $U \in \mathbb{C}^{r \times r}$  and  $V \in \mathbb{C}^{t \times t}$  are unitary and  $D \in \mathbb{R}^{r \times t}$  is diagonal with only real entries. The diagonal entries of  $D$  are the positive square root of the eigenvalues of

$HH'$ . Thus, (2.7.1) can be written as

$$\mathbf{y} = UDV'\mathbf{x} + \mathbf{n}. \quad (2.8.2)$$

Letting  $\tilde{\mathbf{y}} = U'\mathbf{y}$ ,  $\tilde{\mathbf{x}} = V'\mathbf{x}$  and  $\tilde{\mathbf{n}} = U'\mathbf{n}$  (2.8.2) becomes

$$\tilde{\mathbf{y}} = D\tilde{\mathbf{x}} + \tilde{\mathbf{n}}. \quad (2.8.3)$$

As  $U$  and  $V$  are unitary, the distributions of  $\tilde{\mathbf{y}}$ ,  $\tilde{\mathbf{x}}$  and  $\tilde{\mathbf{n}}$  are respectively the same as those of  $\mathbf{y}$ ,  $\mathbf{x}$  and  $\mathbf{n}$ . The original channel  $H$  is now equivalent to a set of parallel channels whose gains are the diagonal entries of  $D$ . Since the rank of  $H$  is limited to  $\min\{r, t\}$ , only  $\min\{r, t\}$  diagonal elements of  $D$  are nonzero. Denoting them by  $\lambda_i$ , the parallel subchannels are

$$\tilde{y}_i = \lambda_i \tilde{x}_i + \tilde{n}_i \quad 1 \leq i \leq \min\{r, t\} \quad (2.8.4)$$

Telatar [7] showed that the optimum (giving maximum channel capacity) power of the  $i$ th subchannel is  $\left(\mu - \frac{1}{\lambda_i^2}\right)^+$  where the parameter  $\mu$  is determined by the total power  $P_t$  such that

$$P_t = \sum_i \left(\mu - \frac{1}{\lambda_i^2}\right)^+. \quad (2.8.5)$$

The notation  $a^+$  denotes  $\max\{0, a\}$ . With this optimum power control, the channel capacity becomes

$$C_{WF} = \sum_i (\log_2 (\mu \lambda_i^2))^+. \quad (2.8.6)$$

Rewriting this in the form of (2.7.5), the capacity is

$$C_{WF} = \log_2 \left[ \det \left( I_r + \frac{1}{\sigma^2} H \tilde{Q} H' \right) \right] \quad (2.8.7)$$

where  $\tilde{Q}_{ii} = \left(\mu - \frac{1}{\lambda_i^2}\right)^+$ . Also we have  $\tilde{Q} = UQU'$ , that implies  $Q = U'\tilde{Q}U$ , the transmit covariance matrix of the original system of (2.7.1).

Finding the value of parameter  $\mu$  from (2.8.5) involves a fair amount of computation. Moreover, if the transmitter's estimation of  $H$  is incorrect (and thus the values  $\lambda_i$ ), then waterfilling can give a worse capacity than the equal power rule. The effect of incorrect channel estimation on waterfilling and capacity has been studied in [8].

## 2.9 Outage Capacity

The capacity described by (2.7.5) or (2.8.7) is instantaneous, for a given realization of channel  $H$ . Since in Rayleigh fading the channel matrix  $H$  changes randomly, the capacity is also random. One way to express the capacity of a such a channel is the ergodic mean of (2.7.5) or (2.8.7). However, this mean capacity is not very useful in terms of the *outage capacity*. Outage capacity is related to the *outage probability*, which is the fraction of time the capacity falls below a given threshold  $C_{outage}$ . The outage probability  $q$  is defined as

$$q = P_r\{C \leq C_{outage}\} \quad (2.9.1)$$

This can also be expressed as

$$1 - q = P_r\{C > C_{outage}\} \quad (2.9.2)$$

A capacity of 20bps/Hz with 1% outage probability means that the capacity will remain at least 20bps/Hz for 99% of the time.

## 2.10 Measurement of Capacity

The theoretical capacities as discussed above are the absolute limit under all ideal conditions. However, a real system can only achieve a portion of that capacity. The *throughput* of a real system is defined as a parallel quantity to express the spectral efficiency of a given system. Here, capacity refers to the absolute achievable limit with the particular system architecture.

A communication system employing MQAM constellations with ideal Nyquist pulses ( $\text{Sinc}[t/T_s]$ ), occupies a bandwidth of  $W = 1/T_s$  and supports a bit rate of  $R = (\log_2 M)/T_s$ . For such an uncoded MQAM system, the throughput, in bps/Hz is  $\log_2 M$ . However, there are errors, and if the transmission is in form of blocks of  $L$  bits, then the effective throughput in terms of the block error rate (BLER) can be written as [10]

$$\begin{aligned} T &= (\log_2 M) \times (1 - \text{BER}) \\ &= (\log_2 M) \times \left(1 - (1 - \text{BER})^L\right). \end{aligned} \quad (2.10.1)$$

Here, BER is the bit error rate of the data stream. For a MIMO system there is more than one substream of data, each of which has a throughput of (2.10.1). The total throughput of the system is then

$$T_{tot} = \sum_{i=1}^n T_i \quad (2.10.2)$$

where  $n$  is the total number of substreams.

## 2.11 Simulation Results

This section shows some plots derived from (2.7.5) and (2.8.7) for different SNRs and  $(r, t)$  pairs. The outage capacity as discussed in section 2.9 can also be expressed in terms of its *cumulative distribution function* (CDF). However, its *complementary cumulative distribution function* (CCDF) is more often used. As an exact closed form expression of the CDF or CCDF is highly involved, this section shows numerically derived capacities of CCDs obtained from Monte-Carlo simulated data.

Fig. 2.5 shows the mean capacity of MIMO systems as a function of SNR for different  $(r, t)$  combinations. The  $(1, 1)$  system capacity is equivalent to the SISO Shannon capacity but for a Rayleigh channel. At high SNR, for a  $(1, 1)$  system the increase in capacity is roughly 1 bit for a 3dB increase in SNR. However, in MIMO, even for a  $(4, 4)$  system, a 3dB increase in SNR results in about 4 bits of increase in capacity. The capacity increase is almost linear in terms of  $(r, t)$ , for  $r = t$ .

The capacity CCDFs are shown in Fig. 2.6 for a system with 0dB SNR. We can see, for example, that for a  $(4, 4)$  system the capacity is about 2.5bps/Hz with 5% outage probability. For a  $(8, 8)$  system this is about 5.8 bps/Hz.

The capacity CCDF as a function of SNR is shown in Fig. 2.7. Only  $(1, 1)$  and  $(4, 4)$  systems are depicted for comparison. We see that at a 5% outage probability level the capacity increase is about 2bps/Hz for every 3dB increase in SNR whereas for the  $(1, 1)$  case the increase is not even visible at low SNRs and is only a fraction of a bit at high SNRs.

The benefit of waterfilling power control is demonstrated in Fig. 2.8. As

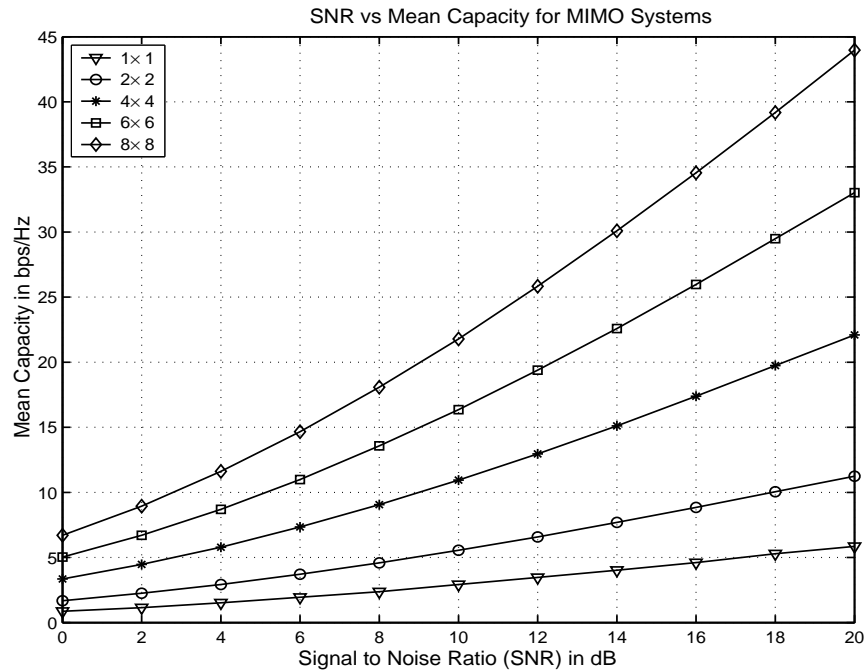


Figure 2.5: Mean capacity of different MIMO systems.

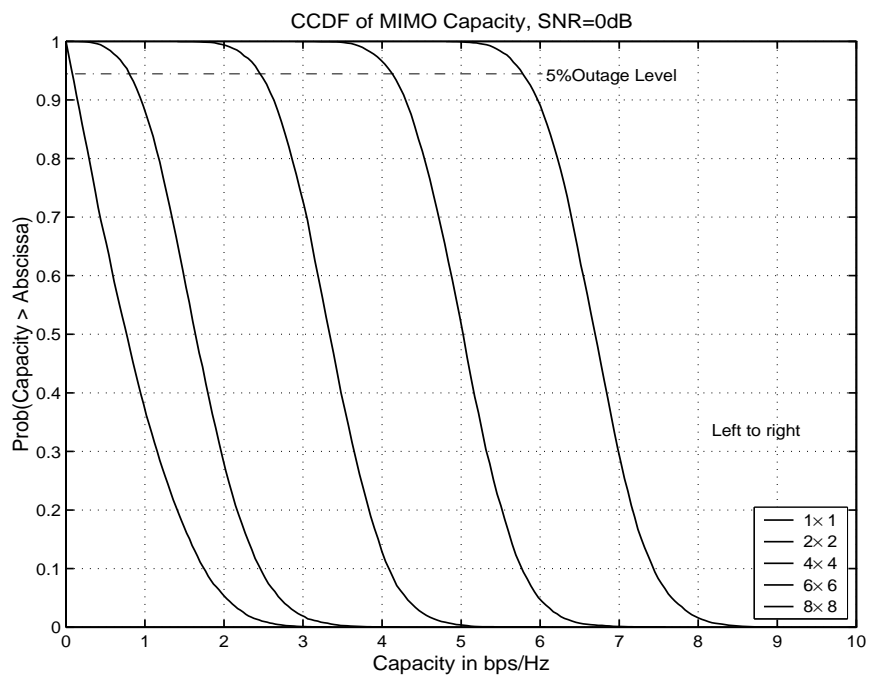


Figure 2.6: Capacity CCDFs of different MIMO systems at SNR = 0dB.

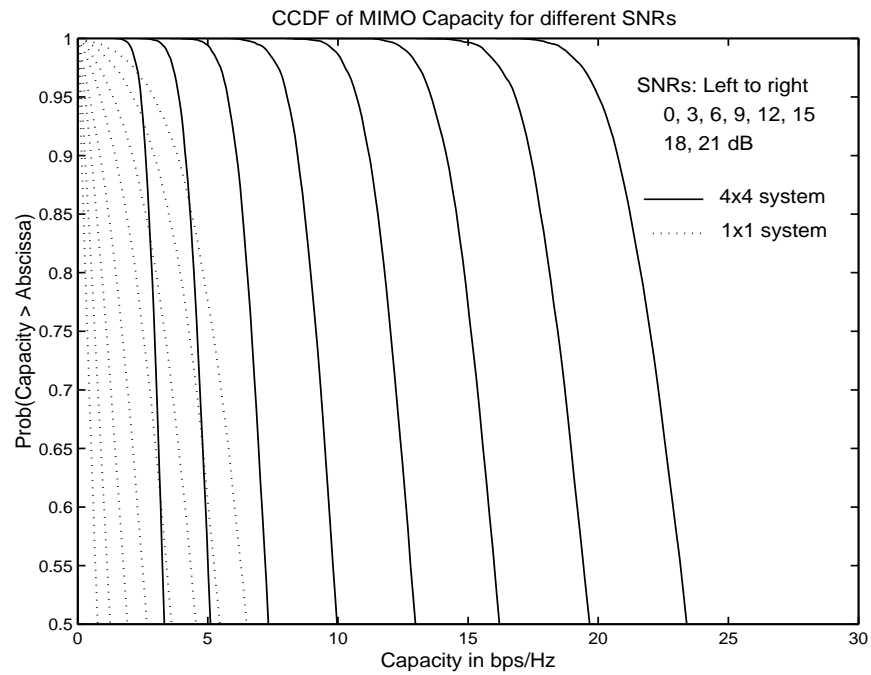


Figure 2.7: MIMO capacity CCDF for different SNRs.

reported by [9], waterfilling is only effective at very low SNRs. For high SNRs power control does not improve the capacity as much as it does for low SNRs.

In producing all of the graphs, *identical and independently distributed* (IID) random channels have been used, and for each trial 10,000 versions of  $H$  have been generated (to average the capacity or to estimate the CCDF.)

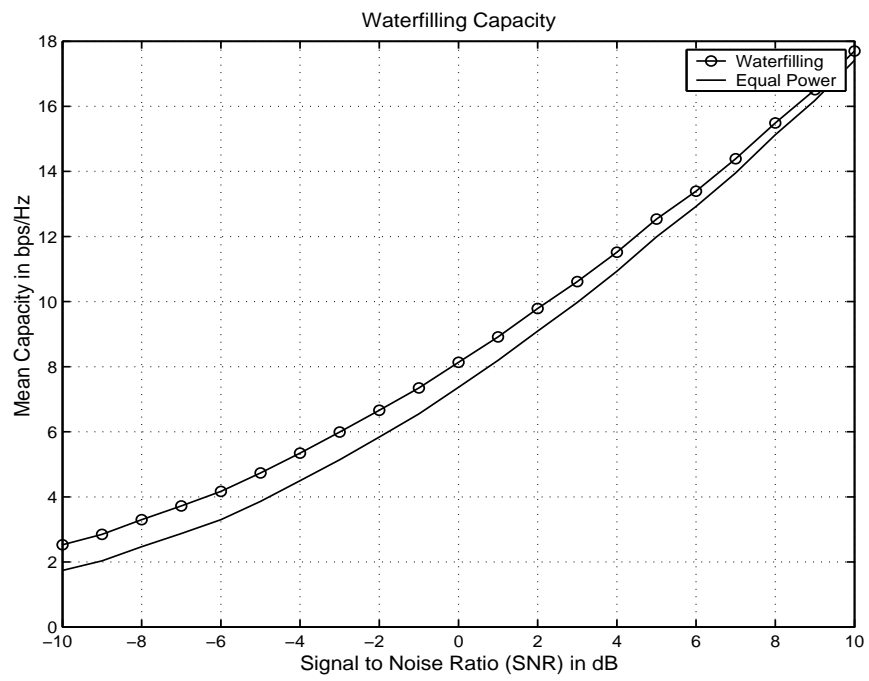


Figure 2.8: MIMO mean capacity with waterfilling, ( $4 \times 4$  system).

# Chapter 3

## Bell Labs Space Time Architecture

### Chapter Outline

This chapter deals with aspects of the VBLAST architecture. Section 3.1 introduces the VBLAST architecture and its operation. The detection method, nulling, interference cancellation and optimal ordering are discussed in sections 3.2 and 3.3. The decoding algorithm is given in section 3.6, and an exact unreported complexity analysis of the decoding algorithm is done in section 3.7. This is one of the contributions of this thesis. Section 3.8 shows VBLAST decoding using the QR decomposition. The benefits of forward and backward sweeps are considered in section 3.9, including ordering for optimal detection in section 3.10. Calculation of complexity are given in section 3.11. The chapter ends with some simulation results showing the performance of the original VBLAST and QR methods.

### 3.1 Introduction

To achieve the high capacities promised by using a MIMO scheme, Foschini et al [11] proposed an architecture known as *Bell Labs Space Time*, BLAST for short. The original BLAST system used a diagonally dispersed coding structure, the implementation of which was technically involved. Instead, a modified version known as *Vertical Bell Labs Space Time*, or VBLAST for short was proposed and prototyped in the laboratory [12]. A simplified block diagram of the VBLAST system is depicted in Fig. 3.1. A single data stream is demultiplexed into  $t$  substreams, and each substream is then encoded into constellation symbols and fed to its respective transmitter. Each transmitter is an ordinary QAM transmitter, and the symbols are taken from a QAM constellation. The encoding process is simply a bit to symbol mapping for each substream, and all substreams are mapped independently. The total transmit power is equally divided among the  $t$  transmitters. The  $r$  receivers are conventional QAM receivers operating independently in the same frequency band. Each receiver receives signals from all the transmitters. The channel matrix  $H$  is assumed quasistationary, meaning it remains constant during the transmission of a whole data block. For this reason, decoding a whole stream is decoding each symbol of that stream. The next section discusses the detection of the individual symbols.

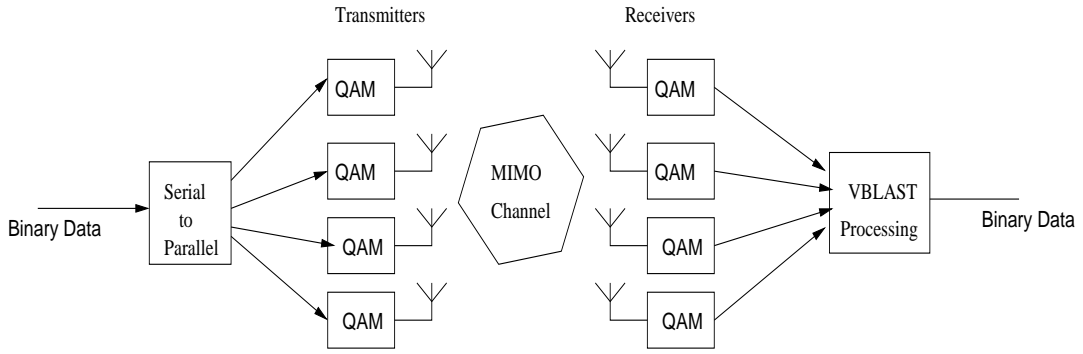


Figure 3.1: The VBLAST architecture.

## 3.2 Detection Process

The detection process of the VBLAST system involves is the estimation of  $\mathbf{x}$  given  $\mathbf{y}$  and  $H$  in

$$\mathbf{y} = H\mathbf{x} + \mathbf{n}. \quad (3.2.1)$$

The  $t$  elements of the transmit vector  $\mathbf{x}$  are constellation symbols which are assumed to be uncorrelated. We also assume that the channel matrix  $H$  is full rank. It is shown later that the second assumption is very crucial to the operation of the VBLAST system. The receiver knows the received vector  $\mathbf{y}$  and has an estimation of  $H$ . The detection process is then a multiuser detection type process. The process involves two steps [13]:

- Slicing (and then decoding) a symbol while nulling the others
- Cancelling the effect of each new decoded symbol from the rest

### 3.2.1 Nulling

Denoting the  $i$ th column of  $H$  as  $\mathbf{h}_i$  the received vector can be written as

$$\mathbf{y} = x_1\mathbf{h}_1 + x_2\mathbf{h}_2 + \cdots + x_t\mathbf{h}_t + \mathbf{n} \quad (3.2.2)$$

here  $x_i$  is the transmitted symbol from the  $i$ th transmit antenna. Nulling is performed by linearly weighting the received symbols to satisfy the *zero forcing* (ZF) or *minimum mean squared error* (MMSE) performance criterion. The zero forcing nulling vector  $\mathbf{w}_i$  is chosen such that

$$\mathbf{w}_i^T \mathbf{h}_j = \begin{cases} 0 & \text{for } i \neq j \\ 1 & \text{for } i = j \end{cases} \quad (3.2.3)$$

where  $()^T$  indicates transpose. Then, the decision statistic for the  $i$ th symbol is

$$\begin{aligned} d_i &= \mathbf{w}_i^T \mathbf{y} \\ &= x_1 \mathbf{w}_i^T \mathbf{h}_1 + x_2 \mathbf{w}_i^T \mathbf{h}_2 + \cdots + x_i \mathbf{w}_i^T \mathbf{h}_i + \cdots + x_t \mathbf{w}_i^T \mathbf{h}_t + \mathbf{w}_i^T \mathbf{n} \\ &= 0 + 0 + \cdots + x_i + \cdots + 0 + \tilde{n}_i \end{aligned} \quad (3.2.4)$$

A soft or hard decision now can be made on  $d_i$  to estimate the the transmitted symbol

$$\hat{x}_i = Q(d_i) \quad (3.2.5)$$

where  $Q(\cdot)$  is the soft/hard decision function.

### 3.2.2 Interference Cancellation

The effect of symbols already detected can be subtracted from the symbols yet to be detected. This improves the overall performance when the order of detection is chosen carefully.

Denoting the received vector  $\mathbf{y}$  by  $\mathbf{y}_1$ , if the nulling vector is  $\mathbf{w}_1$ , then the decision statistic for the 'first' symbol is

$$d_1 = \mathbf{w}_1^T \mathbf{y}_1 \quad (3.2.6)$$

If  $\hat{x}_1 = Q(d_1)$  is the estimated  $x_1$  after the decision (soft or hard), then the interference due to  $\hat{x}_1$  on the other symbols can be subtracted by taking

$$\mathbf{y}_2 = \mathbf{y}_1 - \hat{x}_1 \mathbf{h}_1 \quad (3.2.7)$$

assuming  $\hat{x}_1 = x_1$ , i.e, the decision taken was correct. The next symbol is then detected by finding  $\mathbf{w}_2$  and then making a decision on  $\mathbf{w}_2^T \mathbf{y}_2$  and so on. The performance of this successive cancellation and detection scheme depends on the decision taken on each stage, as any wrong decision is propagated through all the later stages.

### 3.3 Optimal Detection Order

To minimize error propagation the 'strongest' symbols are detected first. This is known to be the optimal detection order.

A simple 'optimal' ordering is based on the postdetection SNR of each substream. The SNR for the  $i$ th detected symbol of vector  $\mathbf{y}$  is given by [13]

$$\rho_i = \frac{E\{|x_i|^2\}}{\sigma^2(\|\mathbf{w}_i\|^2)} \quad (3.3.1)$$

where  $\sigma^2$  is the noise power and  $E\{\}$  denotes the expectation. As  $\|\mathbf{w}_i^T \mathbf{h}_i\|^2 = \|\mathbf{w}_i\|^2 \|\mathbf{h}_i\|^2$ , from (3.2.3) it is seen that a smaller  $\|\mathbf{w}_i\|^2$  value requires the corresponding  $\mathbf{h}_i$  have higher 2-norm. So the SNR in (3.2.7) for the  $i$ th substream is proportional to the norm of the  $i$ th column of  $H$ . Thus, the optimal detection order is in decreasing order of the 2-norm of the columns of  $H$ .

### 3.4 Computing the ZF Nulling Vector

The vector  $\mathbf{w}_i$  in (3.2.3) is unique and is the  $i$ th row of the pseudoinverse of  $H$  [13]

$$\mathbf{w}_i^T = \langle H^+ \rangle_i \quad (3.4.1)$$

where  $\langle \rangle_i$  denotes the  $i$ th row and  $^+$  denotes the pseudoinverse.

With the successive cancellation and decoding,  $\mathbf{w}_i^T$  is chosen as the  $i$ th row of pseudoinverse of  $H$  whose 1 to  $i - 1$  columns are set to zero. This is due to the fact that at the  $i$ th stage the vector  $\mathbf{w}_i$  has to be orthogonal only to  $\mathbf{h}_j$  for  $j = i$  to  $t$ . With optimal ordering, if  $\{k_1, k_2, \dots, k_t\}$  denotes the optimal order, at the  $k_i$ th stage the ZF nulling vector  $\mathbf{w}_{k_i}$  is

$$\mathbf{w}_{k_i}^T = \left\langle H_{k_i-1}^+ \right\rangle_{k_i} \quad (3.4.2)$$

where  $H_{k_i-1}^+$  denotes the matrix obtained from  $H$  by zeroing the columns  $k_1, k_2, \dots, k_{i-1}$ .

### 3.5 Computing the MMSE Nulling Vector

Using the MMSE criterion, the nulling vector  $\mathbf{w}_i^T$  is the  $i$ th row of the matrix

$$G = \left( H'H + \frac{1}{\rho} I \right)^{-1} H' \quad (3.5.1)$$

where  $\rho$  is the SNR [14]. For successive decoding and optimal ordering based on  $G$ , the matrix  $G$  should be computed on each step from the partially zeroed  $H$  as in (3.4.2).

The MMSE criterion always results in better SNR and thus a better performance. But the disadvantages are that the SNR has to be known at the receiver and a matrix inverse needs to be computed.

### 3.6 Detection Algorithm

The full detection algorithm for ZF VBLAST can be described as follows [13]:

- *initialization*

1.  $i \leftarrow 1$

2.  $G_1 = H^+$
3.  $k_1 = \min_j \|\langle G_1 \rangle_j\|^2$

- *iteration*

1.  $\mathbf{w}_{k_i}^T = \langle G_i \rangle_{k_i}$
2.  $d_{k_i} = \mathbf{w}_{k_i}^T \mathbf{y}_i$
3.  $\hat{x}_{k_i} = Q(d_{k_i})$
4.  $\mathbf{y}_{i+1} = \mathbf{y}_i - \hat{x}_{k_i} H_{k_i}$
5.  $G_{i+1} = H_{k_i}^+$
6.  $k_{i+1} = \min_{j \notin \{k_1, k_2, \dots, k_i\}} \|\langle G_{i+1} \rangle_j\|^2$
7.  $i \leftarrow i + 1$

Please note that in step 3 (and 6)  $\min_j \|\langle G_1 \rangle_j\|^2$  is used to pick the strongest symbol.

This is due to the reason that the *row*  $j$  of  $G$ , which has the minimum 2-norm, corresponds to the  $j$ -th *column* of  $H$  which will have the maximum 2-norm.

### 3.7 Complexity Analysis

The algorithm in section 3.6 spends most of its time in steps (5) and (6) where the nulling vectors and optimal ordering are computed, and both of the steps involve the computation of matrix pseudoinverse. Numerically, the most stable way to compute the pseudoinverse is using the Singular Value Decomposition [16]. We consider only multiplications and additions of complex numbers as an operation.

- The complexity of performing the SVD of  $H = U\Sigma V'$  ( $H$  is  $(r \times t)$ ), using the R-SVD algorithm is  $4r^2t + 22t^3$ .
- Computing the pseudoinverse  $G = H^+ = V\Sigma^{-1}U'$  needs  $r^2t + t^2$  complex operations. Because the inverse of the diagonal matrix  $D$  can be done merely in  $\min(r, t)$  operations, so it can be ignored. The first matrix multiplication requires only  $t^2$  operations because  $D^{-1}$  is diagonal. The second multiplication requires  $r^2t$  operations with no need to calculate the transpose. In computing the pseudoinverse, the zero (if any) singular values are left untouched.

So a total of  $5r^2t + 22t^3 + t^2$  complex operations are required to compute the pseudoinverse. Now, steps (5) and (6) are repeated for  $i = 1$  to  $t$ . That means the pseudoinverse is computed for deflated  $H$  with decreasing dimensions  $(r \times (t - k))$ ,  $k = 0, 1, 2, \dots, t - 1$ .

The total complex operations count is

$$\sum_{i=1}^t (5r^2i + 22i^3 + t^2)$$

which after simplification becomes

$$8a^4 + \frac{83}{6}a^3 + \frac{13}{2}a^2 \quad (3.7.1)$$

under the assumption that  $r = t = a$  and consideration of only square or higher exponent terms.

If the MMSE criterion (3.5.1) is used, then the cost of two matrix multiplications, one inversion and one addition comes instead of computing the pseudoinverse. Once again it is assumed the matrix transposes are not computed explicitly. The first

matrix multiplication requires  $t^2r$ , the matrix addition requires  $t^2$  and the matrix inverse needs  $4t^3$  (using Gaussian Elimination) operations. The second matrix multiplication takes  $t^3$  operations. So the operations count for (3.5.1) is  $5t^3 + t^2r + t^2$ . Like before, steps (5) and (6) are repeated for  $t$  times with deflated  $H$ . The total operations count is then

$$\sum_{i=1}^t (5i^3 + i^2r + i^2).$$

Taking the square and higher order terms only and setting  $r = t = a$ , this becomes

$$\frac{19}{12}a^4 + \frac{19}{6}a^3 + \frac{23}{12}a^2. \quad (3.7.2)$$

As a matrix inversion costs less than a pseudoinverse, *the MMSE criterion requires less computation time than the ZF criterion.*

Finding the optimal decoding order (step 6) can use the results of step 5 and does not require computing the pseudoinverse or inverse again. Thus, the complexity of the nulling vector and optimal ordering computation grows as a fourth power of the number of antennas.

### 3.8 QR Decomposition Based Detection

The computational requirements of the VBLAST decoding algorithm are prohibitive. Thus, we now consider other alternative decoding methods based on the QR decomposition, square root decomposition and other decompositions which are less complex and often approximate. In fact, any algorithm for solving a system of linear equations can be used to decode the VBLAST signals. This chapter focuses on the QR detection. Consider the VBLAST transmission equation (3.2.1). For simplicity, let us consider

$r = t = a$ . The channel matrix  $H$  can be QR decomposed:

$$H = QR \quad (3.8.1)$$

where  $Q$  is a unitary and  $R$  is an upper triangular matrix. Then from (3.2.1)

$$\begin{aligned} \tilde{\mathbf{y}} &= Q'\mathbf{y} \\ &= Q'H\mathbf{x} + Q'\mathbf{n} \\ &= Q'(QR)\mathbf{x} + Q'\mathbf{n} \\ &= R\mathbf{x} + \tilde{\mathbf{n}}. \end{aligned} \quad (3.8.2)$$

In explicit matrix form

$$\begin{pmatrix} \tilde{y}_1 \\ \tilde{y}_2 \\ \tilde{y}_3 \\ \vdots \\ \tilde{y}_a \end{pmatrix} = \begin{pmatrix} r_{11} & r_{12} & \cdots & r_{1a} \\ 0 & r_{22} & \cdots & r_{2a} \\ 0 & 0 & \cdots & r_{3a} \\ \vdots & \vdots & \vdots & \vdots \\ 0 & 0 & \cdots & r_{aa} \end{pmatrix} \begin{pmatrix} x_1 \\ x_2 \\ x_3 \\ \vdots \\ x_a \end{pmatrix} + \begin{pmatrix} \tilde{n}_1 \\ \tilde{n}_2 \\ \tilde{n}_3 \\ \vdots \\ \tilde{n}_a \end{pmatrix}. \quad (3.8.3)$$

Then the  $a$ th received symbol is

$$\tilde{y}_a = r_{aa}x_a + \tilde{n}_a. \quad (3.8.4)$$

Hence the  $a$ th decision statistic  $d_a$  is

$$d_a = \frac{1}{r_{aa}}\tilde{y}_a = x_a + \frac{1}{r_{aa}}\tilde{n}_a. \quad (3.8.5)$$

Once a decision (hard or soft) is made on  $d_a$ , it is assumed that the estimate  $\hat{x}_a$  of the actual transmitted symbol  $x_a$  is correct, and thus its effect can be subtracted from yet to be detected symbols. The  $d_{a-1}$ th decision statistic is then (assuming  $\hat{x}_a = x_a$ )

$$\begin{aligned} d_{a-1} &= \frac{1}{r_{a-1,a-1}}(r_{a-1,a-1}x_{a-1} + \tilde{n}_{a-1} + r_{a-1,a}x_a - r_{a-1,a}\hat{x}_a) \\ &= x_{a-1} + \frac{1}{r_{a-1,a-1}}\tilde{n}_{a-1}. \end{aligned} \quad (3.8.6)$$

In general the  $i$ th decision statistic is

$$\begin{aligned} d_i &= \frac{1}{r_{ii}} \left( y_i - \sum_{j=i+1}^a r_{ij} \hat{x}_j \right) \\ &= x_i + \frac{1}{r_{ii}} \tilde{n}_i. \end{aligned} \quad (3.8.7)$$

As the symbols are detected successively, any wrong decision will affect the subsequent decisions.

### 3.9 Backward and Forward Sweeps

To improve the overall performance, Damen et al, [15] have proposed a two-sweep detection scheme where the symbols are detected twice, once by backward substitution as shown in the previous section and then again by forward substitution. Then for a given symbol among the two estimates, the 'better' one is chosen or both are averaged. For a Forward sweep, the channel matrix  $H$  is decomposed into, using QL decomposition

$$H = Q_f L \quad (3.9.1)$$

where  $Q_f$  is unitary (usually different from  $Q$ ) and  $L$  is now a lower triangular matrix.

Following a similar approach to (3.8.2) the received vector is

$$\tilde{\mathbf{y}} = L\mathbf{x} + \tilde{\mathbf{n}}. \quad (3.9.2)$$

In matrix form

$$\begin{pmatrix} \tilde{y}_1 \\ \tilde{y}_2 \\ \tilde{y}_3 \\ \vdots \\ \tilde{y}_a \end{pmatrix} = \begin{pmatrix} l_{11} & 0 & \cdots & 0 \\ l_{21} & l_{22} & \cdots & 0 \\ l_{31} & l_{32} & \cdots & 0 \\ \vdots & \vdots & \vdots & \vdots \\ l_{a1} & l_{a2} & \cdots & l_{aa} \end{pmatrix} \begin{pmatrix} x_1 \\ x_2 \\ x_3 \\ \vdots \\ x_a \end{pmatrix} + \begin{pmatrix} \tilde{n}_1 \\ \tilde{n}_2 \\ \tilde{n}_3 \\ \vdots \\ \tilde{n}_a \end{pmatrix}. \quad (3.9.3)$$

The first received symbol is

$$\tilde{y}_1 = l_{11}x_1 + \tilde{n}_1. \quad (3.9.4)$$

Hence, the first decision statistic  $d_1$  is

$$d_1 = \frac{1}{l_{11}}y_1 = x_1 + \frac{1}{l_{11}}\tilde{n}_1. \quad (3.9.5)$$

The transmitted symbol  $x_1$  is then estimated as  $\hat{x}_1$  from  $d_1$ . Once again, it is assumed that the estimate  $\hat{x}_1$  is correct. The next decision statistic is then (assuming  $\hat{x}_1 = x_1$ )

$$\begin{aligned} d_2 &= \frac{1}{l_{22}}(l_{22}x_2 + \tilde{n}_2 + l_{21}x_1 - l_{21}\hat{x}_1) \\ &= x_2 + \frac{1}{l_{22}}\tilde{n}_2. \end{aligned} \quad (3.9.6)$$

In general the  $i$ th decision statistic is

$$\begin{aligned} d_i &= \frac{1}{l_{ii}} \left( y_i - \sum_{j=1}^{i-1} l_{ij}\hat{x}_j \right) \\ &= x_i + \frac{1}{l_{ii}}\tilde{n}_i. \end{aligned} \quad (3.9.7)$$

### 3.10 Optimal Ordering

Similar to the VBLAST optimal ordering, the optimal way of detecting symbols is in the order of decreasing SNR. In (3.8.2) and (3.9.2) the SNR contribution of the symbol  $x_i$  to the received signal is

$$\|R_i\|^2 \frac{E\{|x_i|^2\}}{\sigma^2} = \|L_i\|^2 \frac{E\{|x_i|^2\}}{\sigma^2} = \|H_i\|^2 \frac{E\{|x_i|^2\}}{\sigma^2} \quad (3.10.1)$$

where  $H_i, R_i$  and  $L_i$  are respectively the  $i$ th columns of  $H, R$  and  $L$  and the notation  $\|\cdot\|^2$  means the 2-norm [15]. Here  $\sigma^2$  is the noise power.  $E\{|x_i|^2\}$  denotes the average symbol energy of the symbol  $x_i$ .

So in the case of a backward sweep the columns of  $R$  should be arranged in increasing order of norm and in the forward sweep the columns of  $L$  should be arranged in decreasing order of norm. The ordering of columns of  $R$  and  $L$  can be done by first permuting the columns of  $H$  and then computing the QR decomposition.

### 3.11 Complexity Analysis of the QR Decoder

As pointed out in [15], in QR decoding most of the time is spent finding the QR factors of the channel matrix. In this study, the Householder method for QR and QL decomposition has been implemented. For  $a \times a$  matrix, the Householder method requires  $\frac{4}{3}a^3$  complex operations to find  $R$  or  $L$  and an extra  $\frac{4}{3}a^3$  to get  $Q$  [16]. So, a total of  $\frac{8}{3}a^3$  operations are required for the whole decomposition. To filter the received vector through  $Q'$  demands an extra  $a^2$  operations. Thus the QR method requires  $\frac{8}{3}a^3 + a^2$  complex operations. For the backward and forward sweeps (QR+QL), twice that number of complex operations  $\frac{16}{3}a^3 + 2a^2$  are needed. The back substitution is not considered here because the VBLAST system also has a similar step which was not considered in finding the complexity of the VBLAST system.

### 3.12 Simulation Results

This section shows some simulation results that determine the different parameters and factors for further simulations. Only IID random channel model is used. The IID random and other MIMO channel models are described in Chapter 6.

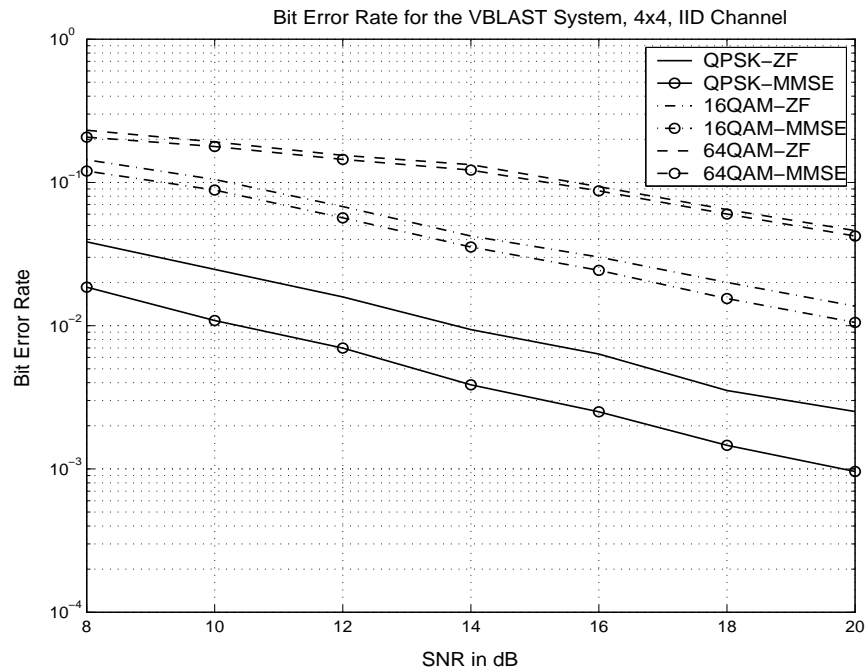


Figure 3.2: Bit error rate of the VBLAST system in IID random channel.

### 3.12.1 BER, BLER and Throughput

Fig. 3.2 shows the BER performance of VBLAST using different constellation sizes. Both the ZF and MMSE criteria are used. The channel model is IID random. It is well known that larger constellation sizes require comparatively higher SNRs for a given BER. We see that 64QAM has the highest BER and QPSK the lowest in Fig. 3.2. Fig. 3.3 shows the probability of a block error. It should be recalled that a block is in error when one or more bits are in error as no form of coding is used. For 64QAM the block error rate is so high that almost every block is in error for moderate SNR.

A high Block Error Rate means a lower throughput. Fig. 3.4 shows the throughput under the same assumptions. As it shows, using a 64QAM constellation does not necessarily result in a high throughput. A smaller constellation like QPSK results in a better throughput because of fewer block errors. As the SNR increases, the QPSK

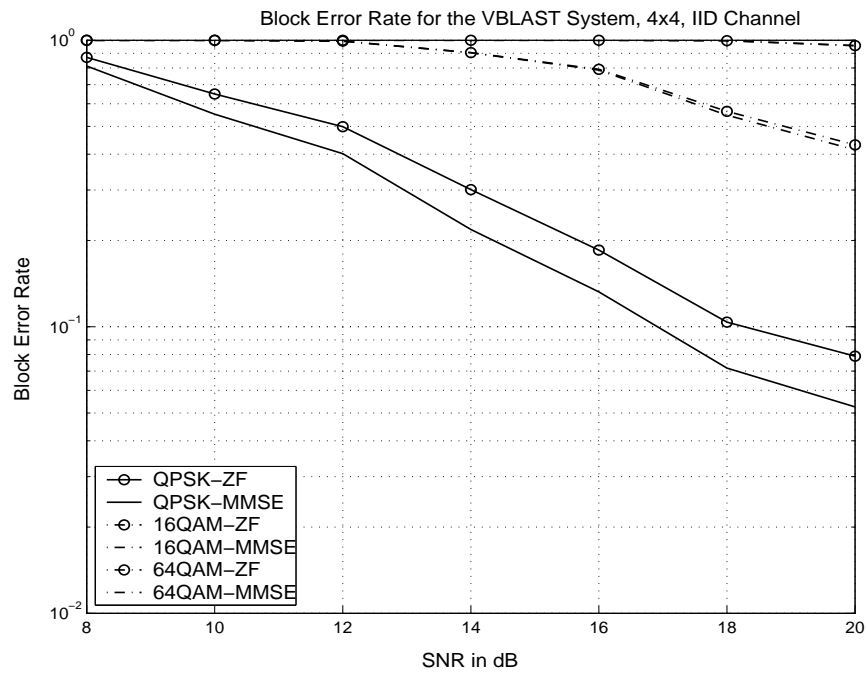


Figure 3.3: Block error rate of the VBLAST system in IID random channel.

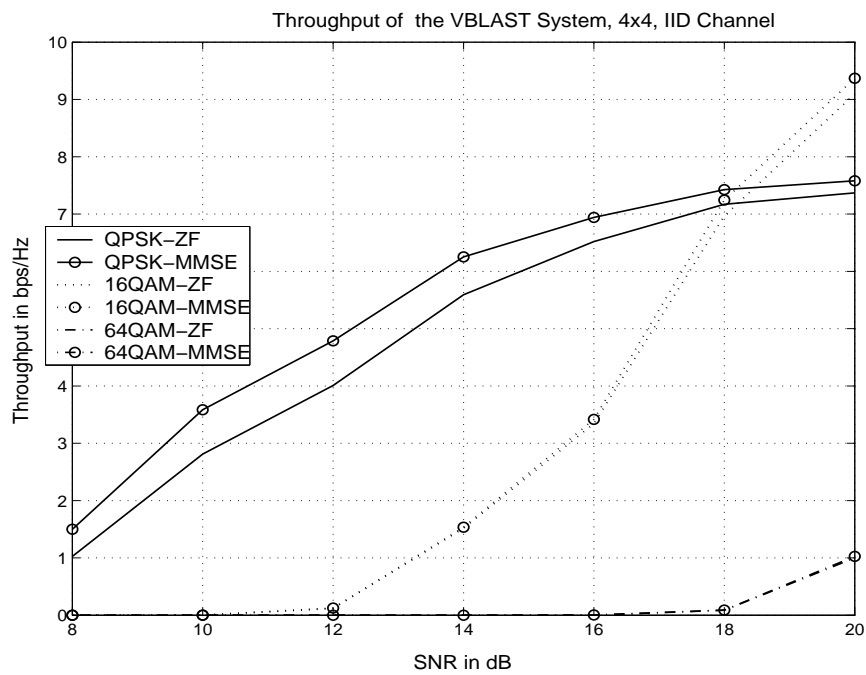


Figure 3.4: Throughput of the VBLAST system in IID random channel.

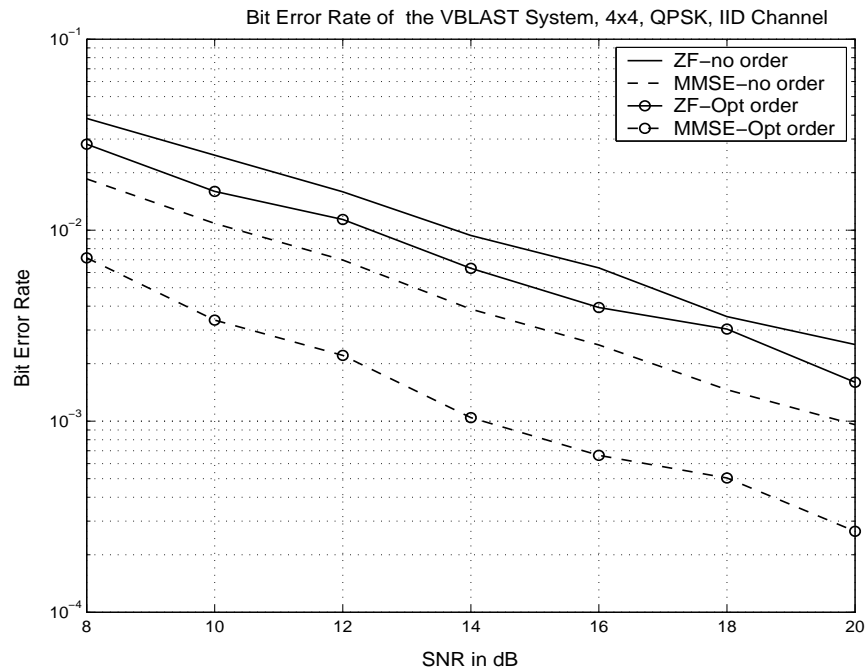


Figure 3.5: Bit error rate of the VBLAST system in IID random channel with optimal ordering.

throughput settles to the maximum for a  $(4 \times 4)$  system. For a given system SNR and target BER, it is tricky to find the optimum constellation size, and a simpler decision is often opted. In this study all subsequent simulations use only QPSK. At an exceptionally high SNR, 64QAM or 16QAM might be used to achieve higher throughput. Another noteworthy point is that the MMSE criterion is only useful at very low SNRs or for smaller constellation sizes.

The effect of optimal ordering is shown in Fig. 3.5. As seen, optimal detection order improves the BER performance by about 2dB for the ZF condition and rises to a significant 5dB using the MMSE criterion.

The BER performance of a QR-based VBLAST system is shown in Fig. 3.6. The use of both backward (QR) and forward (QL) sweeps can help gain an advantage of about 2dB. In this case, the decisions made in each sweep are averaged. Decoding

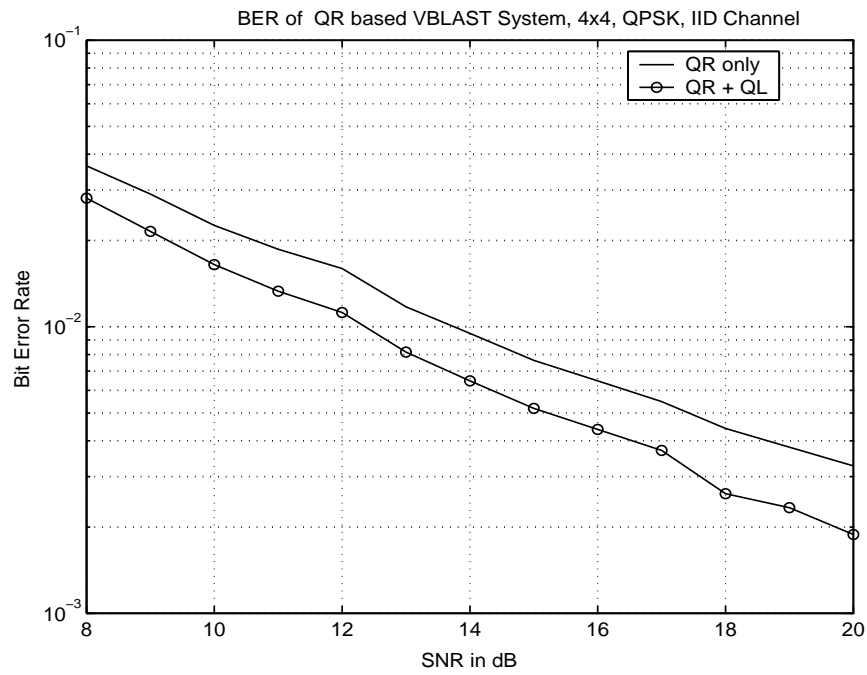


Figure 3.6: Bit error rate of QR based VBLAST system in IID random channel.

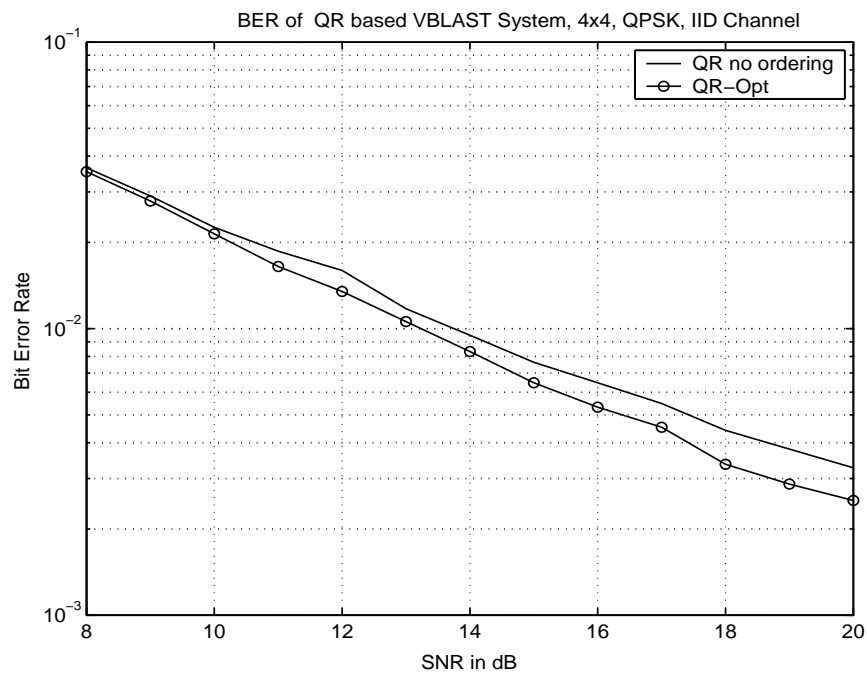


Figure 3.7: Effect of optimal ordering on bit error rate.

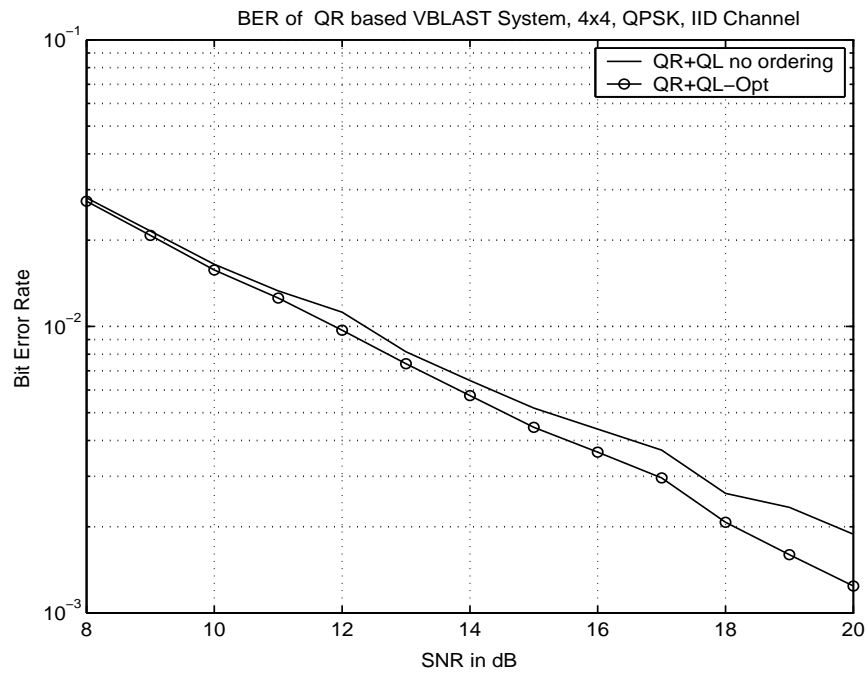


Figure 3.8: Effect of optimal ordering and backward/forward sweep on bit error rate.

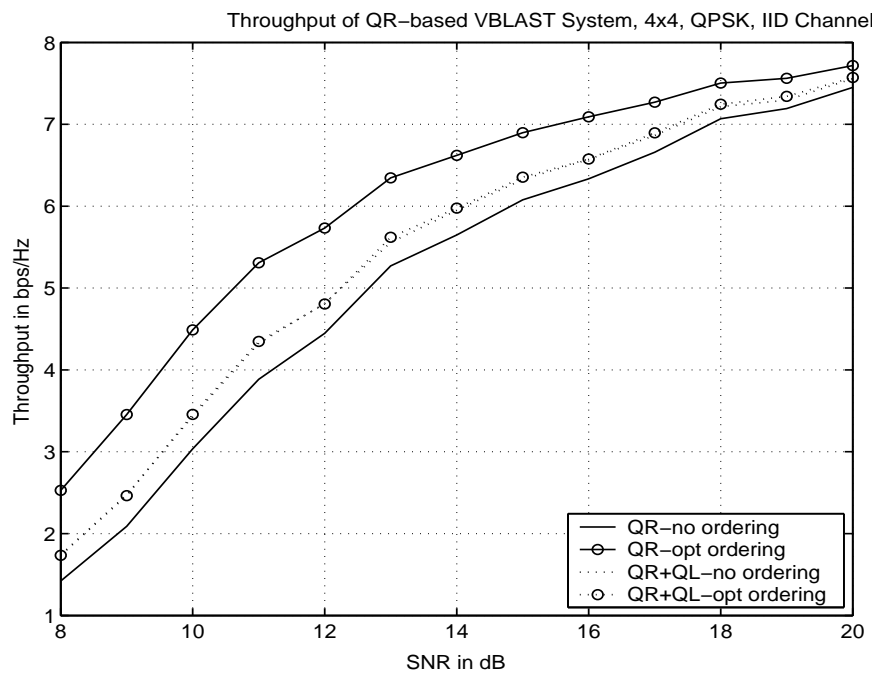


Figure 3.9: Throughput of QR-based VBLAST system.

symbols in the optimal order can also help improve the BERs as shown in Fig. 3.7. However, the combined gain as shown in Fig. 3.8 is not so impressive. Using only the forward sweep and optimal ordering can result in almost the same BER as using both sweeps and optimal ordering. Throughput results are shown in Fig. 3.9.

### 3.12.2 Execution Time

In addition to the BER, BLER and throughput performances, the time required by the VBLAST and VBLAST-QR methods to decode a given amount of transmitted signal are also measured. The theoretical operation counts are plotted in Fig. 3.10. This shows the maximum possible operation count and is an indication of the relative complexity of the two methods. For simulation, the MATLAB software, version 6 was used, which does not allow an operation count. Moreover, the operations count is not a reliable metric to compare algorithms in practice. So the time required by the computer CPU to run the decoding methods was measured. This is shown in Fig. 3.11. As it is seen from the figure, the QR method takes less time than the VBLAST method. The margin of difference is less in Fig. 3.11 than in Fig. 3.10. The reason for this is that the execution time has components (such as memory and disk access) which are common to both methods. In chapter 6, the actual execution times required by these methods are reported. To measure the execution time, 10,000 H and data block of 100 symbols are used.

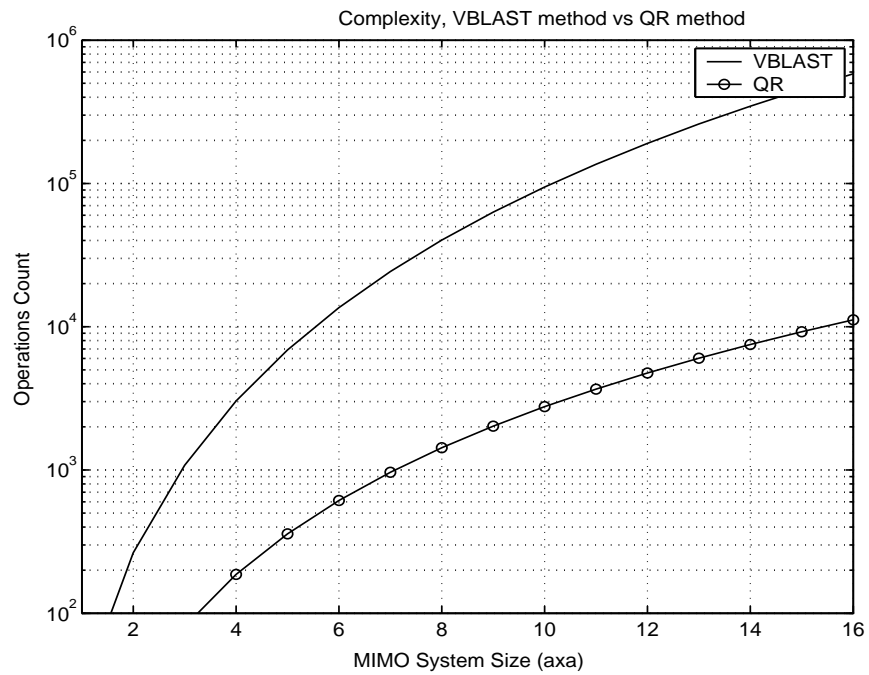


Figure 3.10: Theoretical complexity of the VBLAST and QR methods.

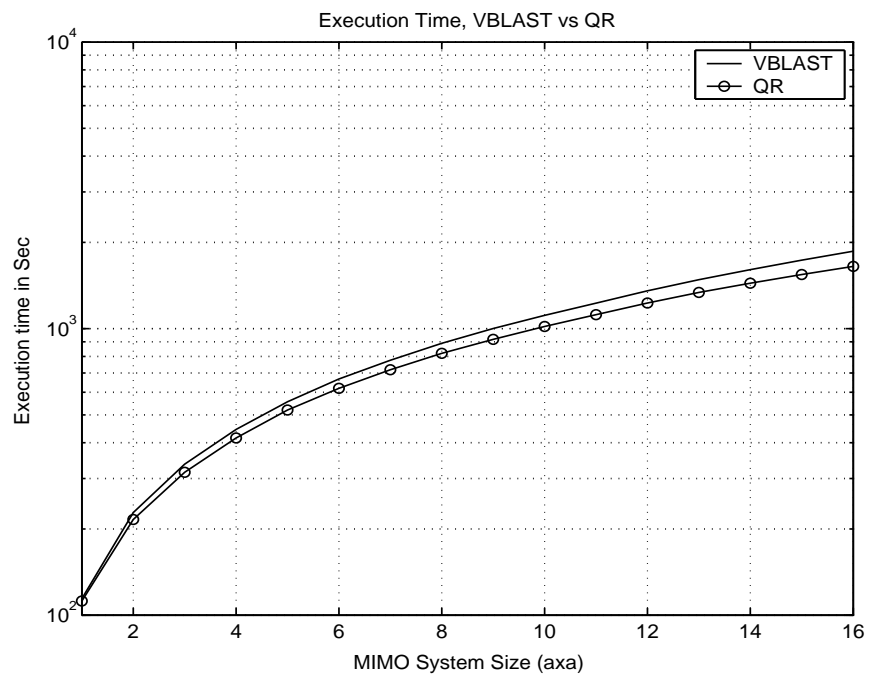


Figure 3.11: Execution time of the VBLAST and QR methods.

# Chapter 4

## New Detection Method for VBLAST

### Chapter Abstract

This chapter is one of the two major contributions of this thesis. The chapter introduces a new detection method for the VBLAST system based on a relatively less known matrix decomposition, the Polar Decomposition (PD). Section 4.1 introduces the PD, and sections 4.2 and 4.3 discuss the use of Cholesky and QR factorizations in addition to the PD for decoding VBLAST signals. The issue of optimal ordering is covered in section 4.4. Section 4.5 lists the properties of the PD, and section 4.6 shows how these properties are conducive to VBLAST detection. Two known algorithms for the PD are reviewed in section 4.7 with complexity analysis in section 4.8. The chapter ends with some simulation results and comments.

## 4.1 The Polar Decomposition

Every matrix  $H \in \mathbb{C}^{r \times t}$  can be expressed as  $H = UP$  with  $U$  unitary and  $P$  positive semidefinite Hermitian. The matrix  $P$  is unique and  $U$  is also unique for a nonsingular  $H$  [17]. This is known as the Polar Decomposition.

Using the Polar Decomposition, the MIMO transmission equation (3.2.1) can be written as

$$\mathbf{y} = UP\mathbf{x} + \mathbf{n}. \quad (4.1.1)$$

Premultiplying both sides by  $U'$ , one finds that

$$U'\mathbf{y} = P\mathbf{x} + U'\mathbf{n} \quad (4.1.2)$$

which is equivalent to

$$\tilde{\mathbf{y}} = P\mathbf{x} + \tilde{\mathbf{n}} \quad (4.1.3)$$

where we have  $\tilde{\mathbf{y}} = U'\mathbf{y}$  and  $\tilde{\mathbf{n}} = U'\mathbf{n}$ . Since,  $U$  is unitary,  $\tilde{\mathbf{y}}$  and  $\tilde{\mathbf{n}}$  have the same distributions as  $\mathbf{y}$  and  $\mathbf{n}$ , respectively.

It is shown later that the equivalent system of (4.1.3) can be solved ( i.e, the transmitted vector  $\mathbf{x}$  can be estimated) with less computational cost if the properties of  $P$  are exploited.

## 4.2 Detection Using the Cholesky Factorization

The Cholesky factorization of a Hermitian positive definite matrix  $P$  is  $P = S'S$  with  $S$  being upper triangular. The inverse of  $S$  can be computed and used to get an upper

triangular system

$$S^{-'} \tilde{\mathbf{y}} = S^{-'} \{S' S \mathbf{x} + \tilde{\mathbf{n}}\} = S \mathbf{x} + \tilde{\tilde{\mathbf{n}}} \quad (4.2.1)$$

where  $S^{-'}$  denotes the Hermitian of the inverse of  $S$  and  $\tilde{\tilde{\mathbf{n}}} = S^{-'} \tilde{\mathbf{n}}$ . Though this process would give the solution, it requires the matrix  $P$  to be nonsingular. The channel matrix  $H$  is often near-rank deficient, and so the Cholesky decomposition is likely to fail occasionally.

### 4.3 Detection Using the QR Factorization

Equation (4.1.3) can also be solved by computing a QR decomposition of the Hermitian matrix  $P = QR$ . With the channel matrix  $H$  decomposed in Polar form and then the matrix  $P$  in  $QR$  form, one writes (3.2.1) as

$$\mathbf{y} = UQR\mathbf{x} + \mathbf{n}. \quad (4.3.1)$$

Filtering the received vector  $\mathbf{y}$  first through  $U'$  and then through  $Q'$ , one has an upper triangular system

$$\tilde{\mathbf{y}} = Q'U'\mathbf{y} = R\mathbf{x} + \tilde{\mathbf{n}}. \quad (4.3.2)$$

In explicit form, letting  $r = t = a$

$$\begin{bmatrix} \tilde{y}_1 \\ \tilde{y}_2 \\ \tilde{y}_3 \\ \vdots \\ \tilde{y}_a \end{bmatrix} = \begin{bmatrix} r_{11} & r_{12} & \cdots & r_{1a} \\ 0 & r_{22} & \cdots & r_{2a} \\ 0 & 0 & \cdots & r_{3a} \\ \vdots & \vdots & \vdots & \vdots \\ 0 & 0 & \cdots & r_{aa} \end{bmatrix} \begin{bmatrix} x_1 \\ x_2 \\ x_3 \\ \vdots \\ x_a \end{bmatrix} + \begin{bmatrix} \tilde{n}_1 \\ \tilde{n}_2 \\ \tilde{n}_3 \\ \vdots \\ \tilde{n}_a \end{bmatrix}. \quad (4.3.3)$$

Then the  $a$ -th received symbol is

$$\tilde{y}_a = r_{aa}x_a + \tilde{n}_a. \quad (4.3.4)$$

Hence the  $a$ -th decision statistic  $d_a$  is

$$d_a = \frac{1}{r_{aa}} \tilde{y}_a = x_a + \frac{1}{r_{aa}} \tilde{n}_a. \quad (4.3.5)$$

Once a decision (hard or soft) is made on  $d_a$ , it is assumed that the decision is correct (i.e, the estimate  $\hat{x}_a$  is the same as  $x_a$ ) and its effect is subtracted from yet to be detected symbols. The  $(a - 1)$ -th decision statistic is then (assuming  $\hat{x}_a = x_a$ )

$$d_{a-1} = x_{a-1} + \frac{1}{r_{a-1,a-1}} \tilde{n}_{a-1}. \quad (4.3.6)$$

In general the  $i$ -th decision statistic is

$$d_i = \frac{1}{r_{ii}} \left( \tilde{y}_i - \sum_{j=i+1}^a r_{ij} \hat{x}_j \right). \quad (4.3.7)$$

## 4.4 Optimal Ordering

Following the same philosophy as VBLAST, the symbols can be detected in order of decreasing SNR. Because the last symbol is detected first in this method, one would like the last symbol to be the best one. This requires rearranging the columns of  $H$  in increasing order of 2-norm (and also the rows of vector  $\mathbf{y}$ ) so that the last symbol corresponding to the last column gets detected first and so on. The optimal ordering can be determined just by comparing the diagonal elements of  $P$ . Because, *the largest diagonal entry of  $P$  corresponds to the strongest symbol.*

## 4.5 Properties of the Polar Decomposition

The main mathematical properties of the Polar Decomposition are [17]

- The Polar Decomposition can be computed from the Singular Value Decomposition. Conversely, given the Polar Decomposition a spectral decomposition of  $P$  will result in the Singular Value Decomposition.
- The unitary matrix  $U$  of the Polar Decomposition is the nearest unitary matrix to  $H$  where the distance is measured using the Frobenius norm.
- The Hermitian matrix  $P$  is the nearest Hermitian positive semidefinite matrix to  $H$  where the distance is measured using 2-norm.

## 4.6 Behavior of Q and P Matrices

One nice feature of the Polar Decomposition is that the matrices  $Q$  and  $P$  do not change abruptly for a slowly varying channel  $H$ . This in contrast to a conventional QR decomposition. Fig. 4.1 shows the relative change in the  $Q$  and  $P$  matrices for a slowly varying channel corresponding to  $F_d T = 0.002$ , a typical indoor environment. This nature of gradual change could enable tracking  $Q$  and  $P$  without requiring repetitive calculation. The possibility of tracking is a subject for further research and is not explored in this study.

## 4.7 Algorithms for the Polar Decomposition

As mentioned above, the Polar Decomposition can be computed from the Singular Value Decomposition. If  $H = U_s D_s V_s'$  is the Singular Value Decomposition and  $H =$

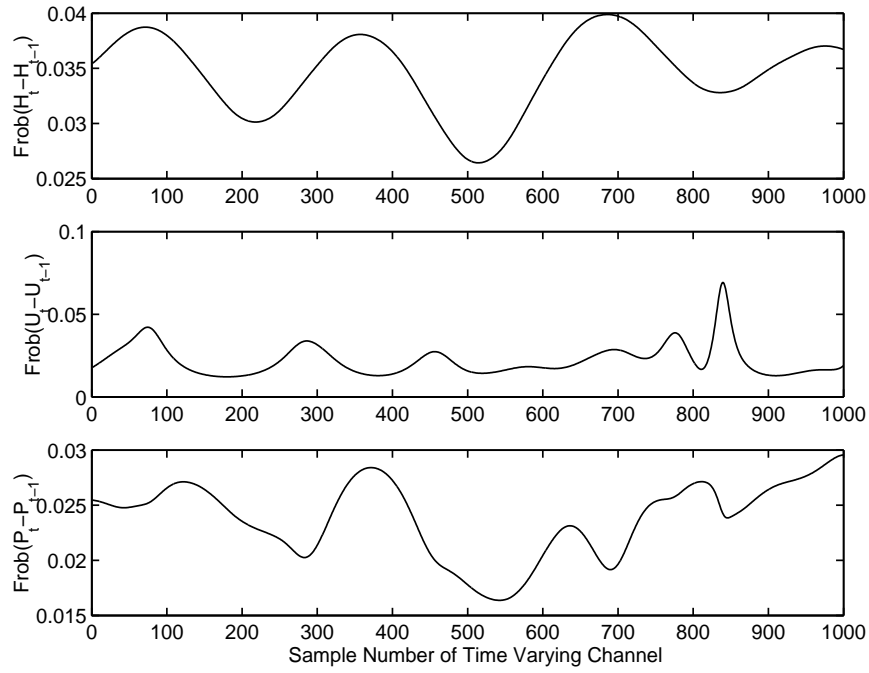


Figure 4.1: Polar Decomposition behavior

$U_p P_p$  is the Polar Decomposition, then  $U_p$  and  $P_p$  can found by

$$\begin{aligned} U_p &= U_s V_s' \\ P_p &= V_s D_s V_s' \end{aligned} \quad (4.7.1)$$

#### 4.7.1 Higham's Algorithm for Polar Decomposition

In addition, there are algorithms that can compute the Polar Decomposition directly from a given matrix. One such algorithm is described by Higham [17] is as follows.

Here  $H$  is the given matrix. It is assumed  $H$  is square and nonsingular. For rectangular and singular matrices the algorithm can be modified. The parameter  $\delta$  is the convergence tolerance.

- *initialization*

1.  $X_0 = H$

2.  $k = -1$

- *iteration*

1.  $k = k + 1$
2.  $\gamma_k = \left( \frac{\|X_k^{-1}\|_1 \|X_k^{-1}\|_{\text{inf}}}{\|X_k\|_1 \|X_k\|_{\text{inf}}} \right)^{\frac{1}{4}}$
3.  $X_{k+1} = \frac{1}{2} \left( \gamma_k X_k + X_k^{-'} / \gamma_k \right)$
4. **until**  $\|X_{k+1} - X_k\|_1 \leq \delta \|X_{k+1}\|_1$
5.  $U = X_{k+1}$
6.  $P = \frac{1}{2} (U^* H + H^* U)$
7. **go to step 1**

The algorithm is based on the classical Newton's iteration to find the square root of a number. With the initialization  $X_0 = H$ , the new  $X_k$  is computed as

$$X_{k+1} = \frac{1}{2} \left( \gamma_k X_k + X_k^{-'} / \gamma_k \right). \quad (4.7.2)$$

Here  $\gamma_k$  is just an acceleration parameter. The convergence analysis of this algorithm is given in [19].

This iterative algorithm converges within 10 to 11 iterations. A modification of this algorithm was later proposed in [18] also by Higham. The new algorithm has better convergence with fewer iterations. Dubrulle [20] reported an optimum iteration that ensures monotonic convergence. Monotonic convergence is very important in the software implementation of a numerical algorithm.

## 4.8 Complexity Analysis

The main computational burden of the proposed method lies in the computation of the Polar Decomposition and the QR factorization. The Polar Decomposition can be found from the SVD of  $H$  with a cost of  $22a^3$  operations assuming the SVD is computed using the Golub-Reinsch algorithm (R-SVD costs  $26a^3$ ). The direct iterative algorithm for Polar Decomposition due to Higham [18] converges in an average of 8 iterations spending  $8a^3$  complex operations. This study uses the Higham method. On top of this, the QR factorization costs  $2a^3$  operations while the filtering by  $U'$  and  $Q'$  can be done merely at a cost of  $2a^2$  operations. The operations in the back substitutions in (4.4.2) are not counted because the VBLAST method has a similar computation which is ignored. So the total cost of this method is expected to be  $10a^3 + 2a^2$ .

## 4.9 Simulation Results

### 4.9.1 BER, BLER and Throughput

The BER performance of the Polar Decomposition-based VBLAST is shown in Fig. 4.2. As seen, the optimal ordering, here also, produces slightly better BER. The Block Error Rate and Throughput are shown in Figs. 4.3 and 4.4 respectively. Further results are given in Chapter 6.

One thing that needs to be mentioned here is that the BER, BLER and throughput of the original VBLAST method are exactly the same as those shown in Fig 4.2 through 4.4. This suggests a mathematical equivalence between the original VBLAST decoding method based on repetitive pseudoinverses and this method based on the

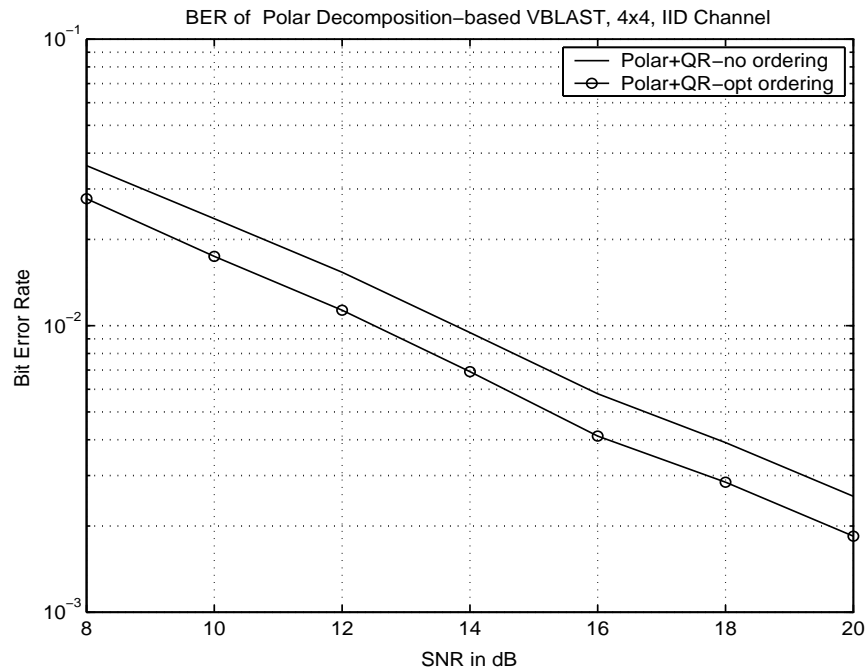


Figure 4.2: Bit error rate of Polar Decomposition-based VBLAST.

Polar Decomposition.

#### 4.9.2 Execution Time

The complexities of the original VBLAST decoding method and the method based on the Polar Decomposition are plotted in Fig. 4.5. These are the theoretical figures and represent the worst case scenario. The execution time of both methods are shown in Fig. 4.6. We just saw that in theory the proposed method based on the Polar Decomposition is less complex and requires less time. The large margin between these two methods as seen in Fig. 4.5 is actually not so large in practice as shown in Fig. 4.6. This is because the real execution time shown in Fig. 4.6 is not just computation time, meaning the execution time also includes time due to memory accesses, disk accesses etc. Contributions due to these non-computation components are common to both, reducing the gap between the two methods.

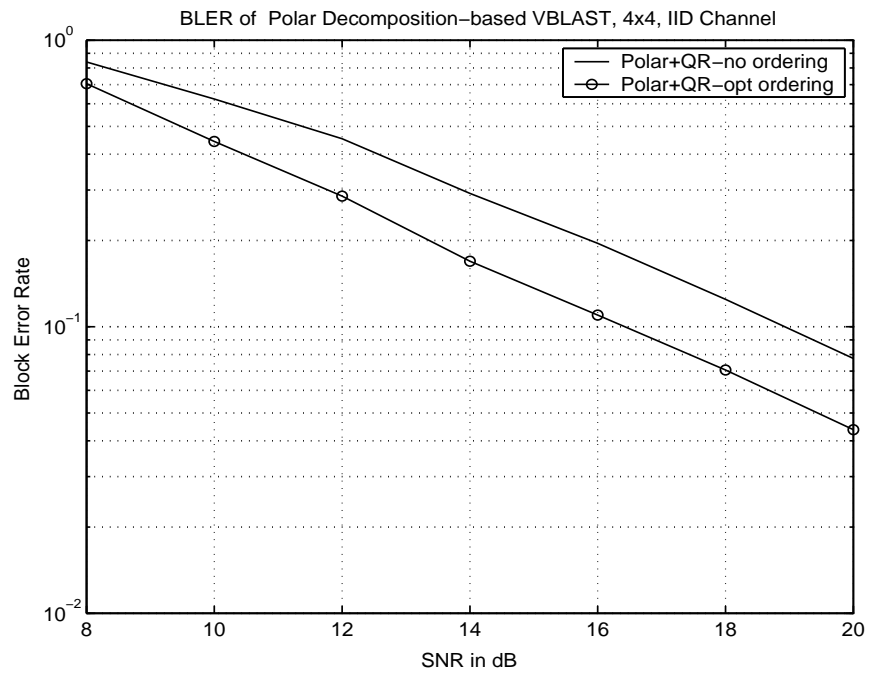


Figure 4.3: Block error rate of Polar Decomposition-based VBLAST.

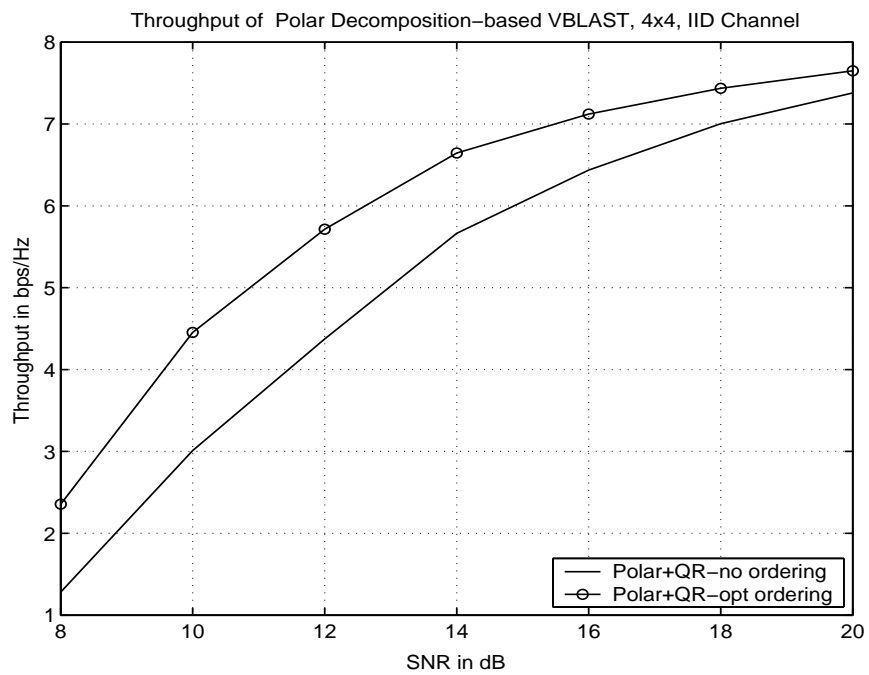


Figure 4.4: Throughput of Polar Decomposition-based VBLAST.

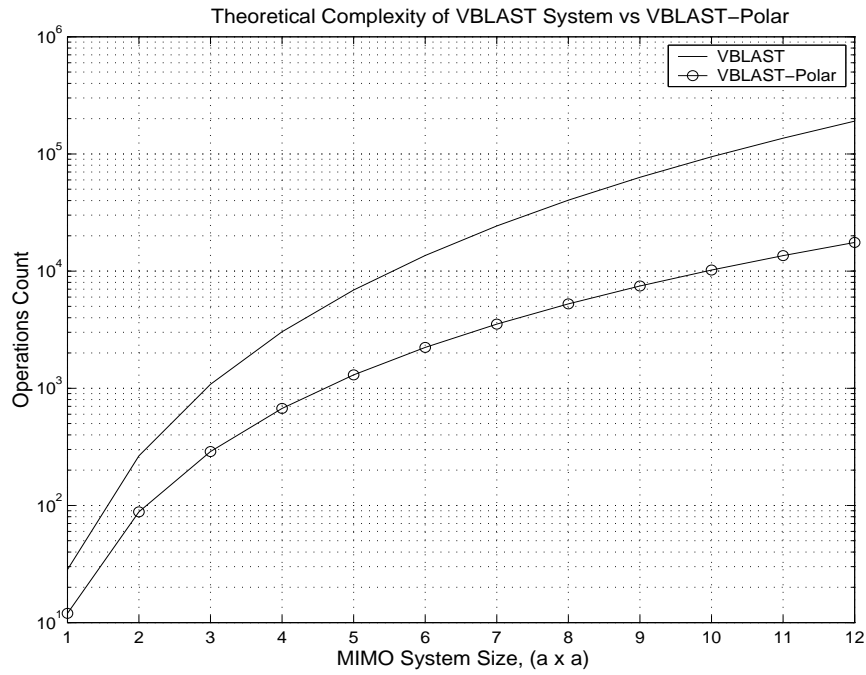


Figure 4.5: Complexity of VBLAST and Polar Decomposition-based VBLAST.

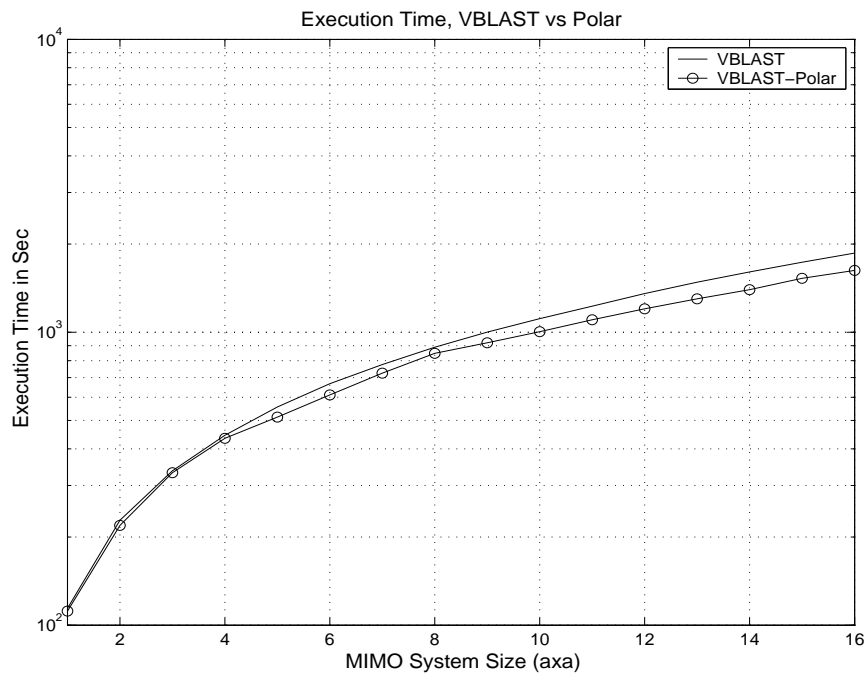


Figure 4.6: Execution time of VBLAST and Polar Decomposition-based VBLAST.

## **Chapter 5**

# **Singular Value Decomposition Based MIMO Systems**

### **Chapter Abstract**

This chapter introduces the Singular Value Decomposition (SVD) based MIMO system. Such systems are suitable for a Time Division Duplex (TDD) mode of communication and can get very close to the theoretical capacity limit. The detailed architecture and properties of the SVD are discussed. The SVD produces subchannels with different gains, and adaptive modulation is used across them. Power control issues are also addressed. The chapter concludes with some simulation results and comments.

## 5.1 Introduction

The Singular Value Decomposition (SVD) of a matrix  $H$  is  $H = UDV'$ , where  $U$  and  $V$  are unitary and  $D$  is a diagonal matrix with positive real elements. The matrix  $H$  is not required to be square to have an SVD. The elements of  $D$  are said to be the singular values of the matrix  $H$ . These elements are also the positive square roots of the eigenvalues of the matrix  $HH'$  or  $H'H$ .

## 5.2 SVD Based MIMO Systems

In a Time Division Duplex channel, the channel information is available at both ends of the communication link within a reasonable accuracy. SVD systems use this channel information to compute the SVD. The transmitter filters vector  $\mathbf{x}$  through  $V$  before sending it over the channel. At the receiver, vector  $\mathbf{y}$  and filters using  $U'$ . The overall transmission equation thus becomes

$$\begin{aligned} U'\mathbf{y} = \tilde{\mathbf{y}} &= U'(H)V\mathbf{x} + U'\mathbf{n} \\ &= U'(UDV')V\mathbf{x} + \tilde{\mathbf{n}} \\ &= D\mathbf{x} + \tilde{\mathbf{n}}. \end{aligned} \tag{5.2.1}$$

As  $D$  is a diagonal matrix, one can write this component-wise as

$$\tilde{y}_i = D_{ii}x_i + \tilde{n}_i. \tag{5.2.2}$$

By denoting the singular values by  $\lambda_i$ , this becomes

$$\tilde{y}_i = \lambda_i x_i + \tilde{n}_i. \tag{5.2.3}$$

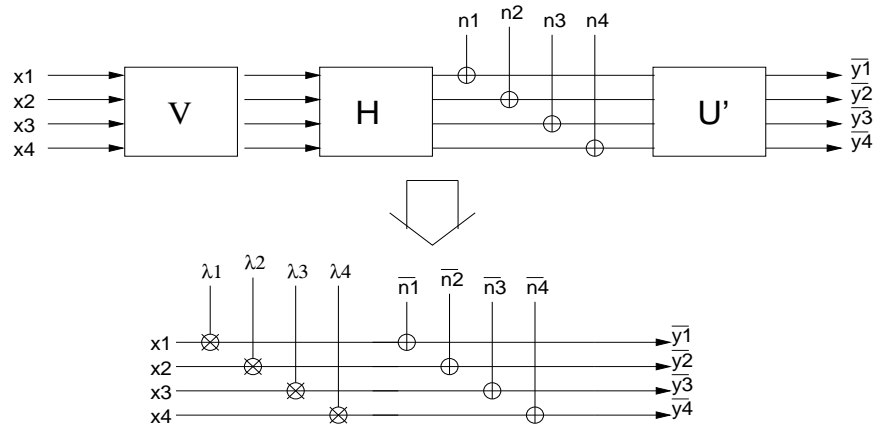


Figure 5.1: SVD-based MIMO transmission scheme.

The original MIMO system of (3.2.1) has now become an equivalent system having a set of parallel subchannels with gains  $\lambda_i$  as shown in Fig. 5.1. The number of subchannels depends on the minimum of  $(r, t)$  without exceeding the rank of the channel matrix  $H$ . As the noise  $n_i$  is assumed to be Gaussian, noise  $\tilde{n}_i$  is also Gaussian after the unitary transformation. The singular values  $\lambda_i$  are sorted in decreasing order of values, and the equivalent parallel subchannels have unequal gains.

A practical implementation of such a system has been reported in [21] and is shown in Fig. 5.2. For this implementation, if the transceiver A needs to transmit some data, it 'asks' B to send pilots. Receiving the pilots PB1 sent by B, A performs the SVD and uses the  $V$  matrix to transmit data at next time slot. A also sends pilots PA1 to enable the transceiver B to transmit. However, one obvious problem is the time delay between two slots. If  $T$  is the time delay, a transceiver has to use  $V_{0-T}$  instead of  $V_0$ . This problem can be solved using a linear filter at the receiver with the aid of the second set of pilots PA2. Details can be found in [22].



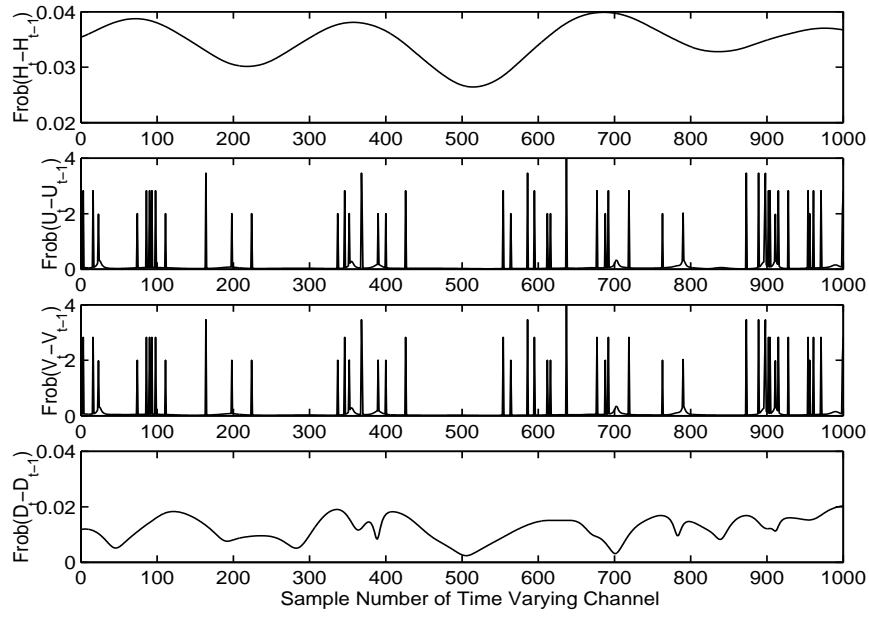


Figure 5.3: Changes in U, V and D matrices for a slowly varying channel matrix H.

## 5.4 SNR of Parallel Subchannels

Since the different subchannels of the SVD system have different gains, the use of different constellation sizes for each subchannel is a good way of achieving higher throughput. However, to implement this, we need to know the SNR of each subchannel.

From (5.2.3), we have the received power

$$E\{|\tilde{y}_i|^2\} = \lambda_i^2 E\{|x_i|^2\} + E\{|\tilde{n}_i|^2\} \quad (5.4.1)$$

where we have used the fact that  $x_i$  and  $\tilde{n}_i$  are statistically independent. In the above equation the received signal power is  $\lambda_i^2 E\{|x_i|^2\}$  and the noise power is  $E\{|\tilde{n}_i|^2\} = \sigma^2$ .

The SNR for the  $i$ th subchannel is then

$$\rho_i = \frac{\lambda_i^2 E\{|x_i|^2\}}{\sigma^2}. \quad (5.4.2)$$

The transmit symbol power  $E\{|x_i|^2\}$  is dependent on the power allocation strategy.

This SNR can then be used to adapt the constellation size following the method

described in section 2.8.

## 5.5 Power Control

The waterfilling method is the ideal power control strategy for SVD Systems, but it requires information about the noise at the transmitter side. Once the total available power, estimates of the noise and gains of the parallel subchannels are known, Telatar [7] showed that the optimum power of the  $i$ th subchannel is  $\left(\mu - \frac{1}{\lambda_i^2}\right)^+$ . The waterfilling parameter  $\mu$  is determined by the total power  $P_t$ , such that

$$P_t = \sum_i \left(\mu - \frac{1}{\lambda_i^2}\right)^+ . \quad (5.5.1)$$

Again, the notation  $a^+$  denotes  $\max\{0, a\}$ . The value of the parameter  $\mu$  can be found by an iterative loop allocating power to all good subchannels. The following MATLAB code snippet finds the parameter  $\mu$ .

```
[u, Sigma, v] = svd(H);
Lamda = diag(real(Sigma).^2);
mu = 0;
K = sum(Lamda ~= 0);
f = 1;
while mu < 1/Lamda(f);
    f = K;
    s = 0;
    for t=1:K;
        s = s + 1/Lamda(t);
    end;

    mu = (Pt + s)/K;
    K = K-1;
end;
```

## 5.6 Adaptive Modulation across Subchannels

As the different subchannels of the SVD system have different gains, each subchannel should use a different constellation size. This decision can be a once off system design parameter which does not change with the time varying channel. On the other hand, the decision can be taken based on the slowly varying channel as well as on the individual subchannel. The latter scheme is used in this study with a truncated waterfilling power control strategy. The truncated power control strategy is the same as original waterfilling except that it does not allocate any power to subchannels with an SNR below a given threshold which is set using the minimum SNR required for QPSK transmission with a desired performance. Any subchannel SNR which falls below the threshold is not used in the transmission and its power is redistributed among the other subchannels. The constellation sizes used in this study are: QPSK, 16QAM and 64QAM. Data are transmitted in the form of fixed-sized blocks, and each subchannel of a block has symbols from constellation of different sizes. Each block has a small header containing the modulation information so that the receiver can properly decode the subchannels.

## 5.7 Simulation Results

The BER of a simulated SVD system is shown in Fig. 5.4. The fixed QPSK curve uses the same modulation on each subchannel. The adaptive and adaptive plus waterfilling (wf) are expected to be flat in the ideal adaptation case. They are not flat as the adaptation is not perfect. The merit of using adaptive modulation becomes clear in

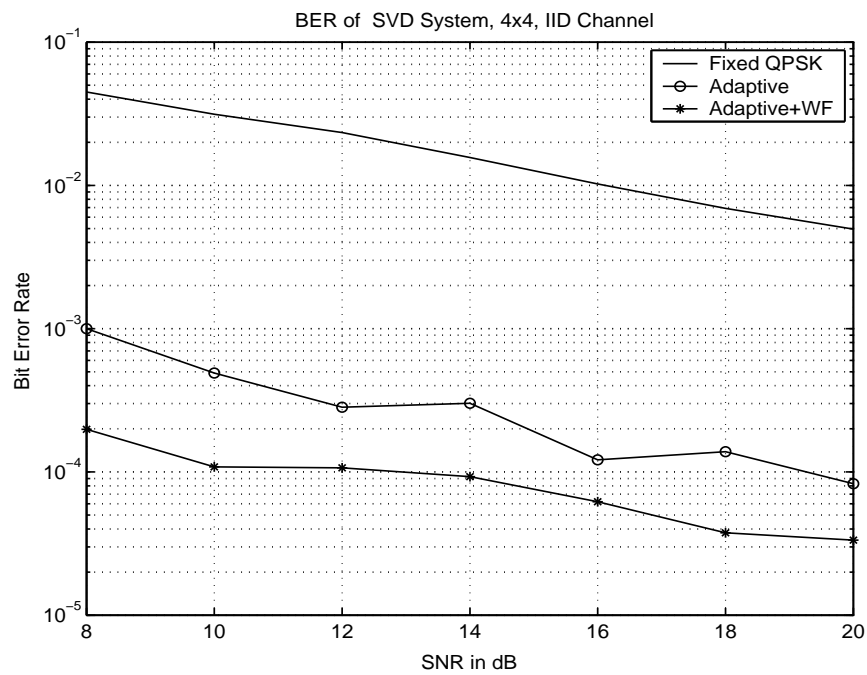


Figure 5.4: Bit error rate of the SVD system.

the throughput shown in Fig. 5.5. Clearly, the adaptive system has a much higher throughput than the fixed system, and combined with the waterfilling power control, further increases the throughput by one bit. These results are compared with those for VBLAST in Chapter 6.

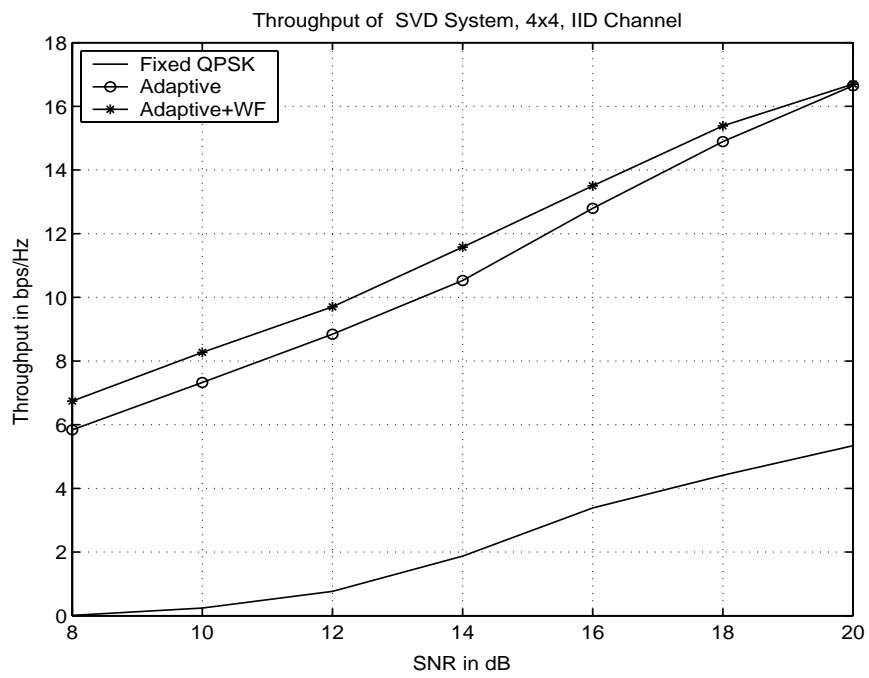


Figure 5.5: Throughput of the SVD system.

# Chapter 6

## Performance Comparison Results

### 6.1 Introduction

This chapter is devoted to simulation results. There are two sets of simulations. One set compares different decoding methods for VBLAST and shows that the Polar Decomposition based decoding method is better than other methods in terms of execution time and BER. In the second set of simulations, the VBLAST system is compared with the SVD based system. For this latter comparison, three types of channel model are considered: an IID (independently and identically distributed) random channel, a slow fading Rayleigh channel and a physical channel measured by the VUT MIMO group. It should be remembered that the VBLAST and SVD systems have different architectures and modes of operation. Table 6.1 shows the acronyms used in the text for the respective MIMO systems.

In addition to these acronyms, the suffix 'opt' will mean optimal decoding order and 'wf' will mean waterfilling power control. Where not specified, equal power control is used and the decoding order is the original order.

Acronym	MIMO System
VBLAST-ZF	VBLAST with ZF nulling vector
VBLAST-MMSE	VBLAST with MMSE nulling vector
VBLAST-QR	VBLAST with QR decoding
VBLAST-QRQL	VBLAST with both QR and QL decoding
VBLAST-PD-QR	VBLAST with PD (plus QR) decoding
SVD	SVD based system with fixed constellation
SVD-MQAM	SVD based system with adaptive constellation

Table 6.1: Acronyms used to denote different MIMO systems.

## 6.2 Channel Models

### 6.2.1 IID Channels

The MIMO IID channels are matrices with every element representing the gain between a pair of receiving and transmitting antennas. Each element is a complex number with both real and imaginary parts being drawn from zero mean,  $\sigma^2 = \frac{1}{2}$  Gaussian distributions. Each channel matrix represents a time snapshot of the physical channel being modelled. For each simulation a minimum of 10,000 channel matrices are generated for each of the MIMO systems developed. Data is transmitted in blocks of 100 vector symbols with each vector having  $n_t$  (number of transmitting antennas) symbols. Each symbol represents a few bits depending on the constellation in use. For these simulations a  $4 \times 4$  system is used, but the results can be extended to system of any dimension.

The noise is modelled as complex white Gaussian with real and imaginary parts being independent, zero mean and with  $\sigma^2 = \frac{1}{2}$ . Thus the complex noise has unit power. The system SNR is a given parameter and is the ratio of the *transmitted power* to the noise. The transmitted signals are normalized so that each antenna transmits unity power (total transmitted power is  $n_t$ ). The power of the noise is adjusted in

accordance with the SNR. Some receivers may need to have an estimate of the SNR for MMSE decoding.

### 6.2.2 Slow Fading Rayleigh Channel

To generate a slow fading channel, a simulator is used, coded by Dr. Reza Berangi of VUT. The simulator is based on the famous Clarke [23] model and asks for  $F_dT$  and the number of channel samples required. The simulator first generates SISO (single input single output) samples. The MIMO matrix channel is then formed using a SISO channel as each element of the matrix. Thus, each element of the MIMO channel matrix fades over time.  $F_dT$  values considered in this study are: 0.002, 0.01 and 0.05 sec, representing terminal speeds of 10cm/sec, 52cm/sec and 2.6m/sec at 5.8GHz and  $T=1\text{ms}$ .

### 6.2.3 VUT Measured Channel

The MIMO group working at VUT has ongoing channel measurement activities [24]. The measurement data are used within and outside of the MIMO group. For this study only two points are chosen from the measured channel: one with obvious line of sight (LOS) path and one with no obvious LOS, corresponding to points A and B in Fig. 6.1, respectively. The details of the measurement setup can be found in [25].

## 6.3 Variants of VBLAST

In this simulation the performances of different decoding algorithms proposed for decoding the VBLAST signals are compared. The decoding methods include the original

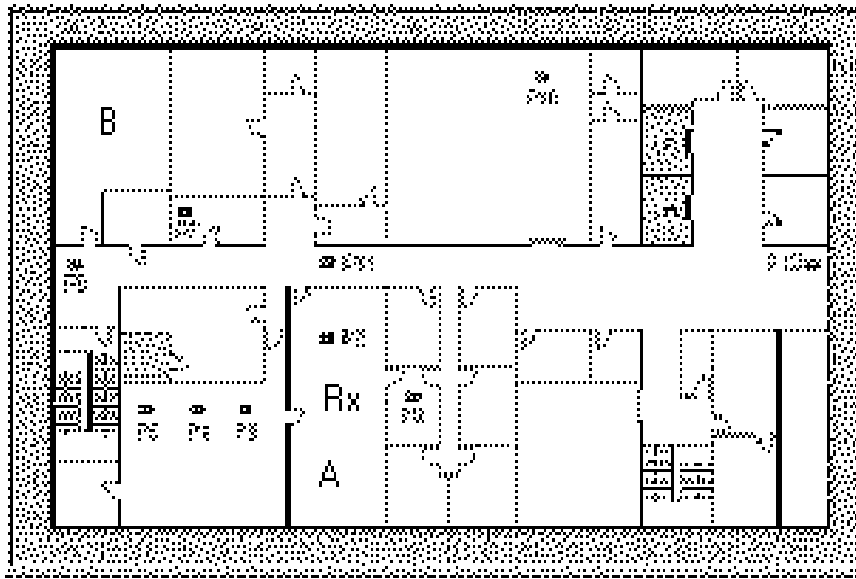


Figure 6.1: Floor map of the measurement. Rx is receiver position, A is LOS point and B is NLOS point.

VBLAST method (chapter 3), methods based on the QR and QL decompositions (chapter 3) and the new method based on the Polar Decomposition (chapter 4). The bit error rate (BER), block error rate (BLER), throughput and execution time are used as the criteria for comparison. The IID random channel model is used for this simulation. We found that for the other channel models the relative performances of the different methods remained the same.

### 6.3.1 BER, BLER and Throughputs

Fig. 6.2 shows the BER for all of the decoding methods. The first thing that is evident from Fig. 6.2 is that the QR method performs within 2 to 3dB of the original VBLAST decoding method in terms of bit error rate. However, using both backward and forward sweeps (i.e, QR and QL) can significantly improve the BER, yielding a performance

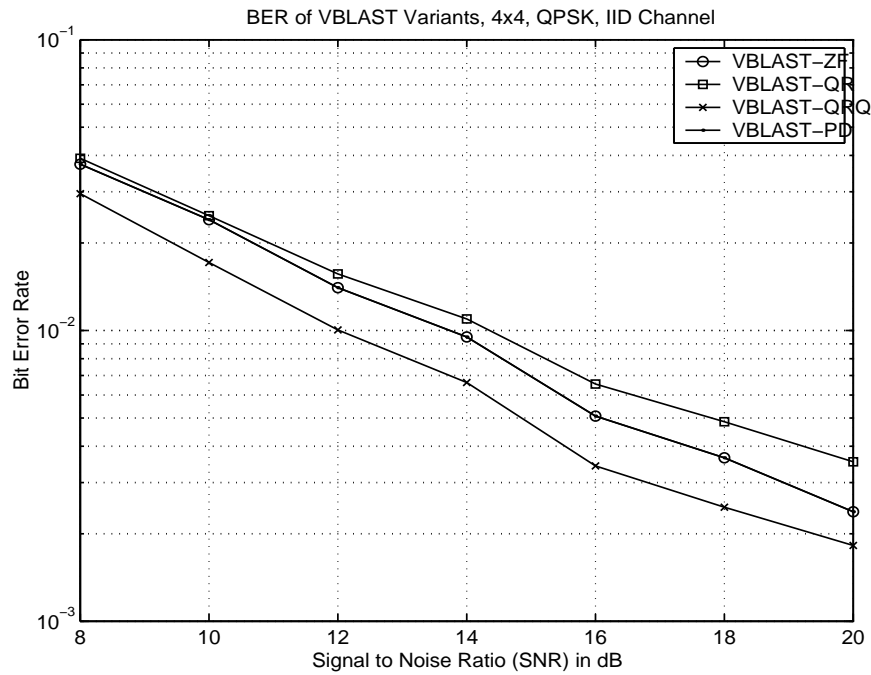


Figure 6.2: Bit error rate of VBLAST for different decoding methods.

substantially better than the VBLAST method. On the other hand the Polar Decomposition based decoding has **exactly the same** BER as the original VBLAST. This interesting result leads us to believe that there is some form of mathematical equivalence between the VBLAST decoding method and the proposed Polar Decomposition based method. The veracity of this statement is yet to be established mathematically, but extensive simulations confirmed the claim.

The BERs reported in Fig. 6.2 are without using any particular decoding order. Using the optimal order as discussed in earlier chapters produces the results given in Fig. 6.3.

With the optimal decoding order the results are similar. Once again the original VBLAST method and VBLAST method based on the Polar Decomposition produce

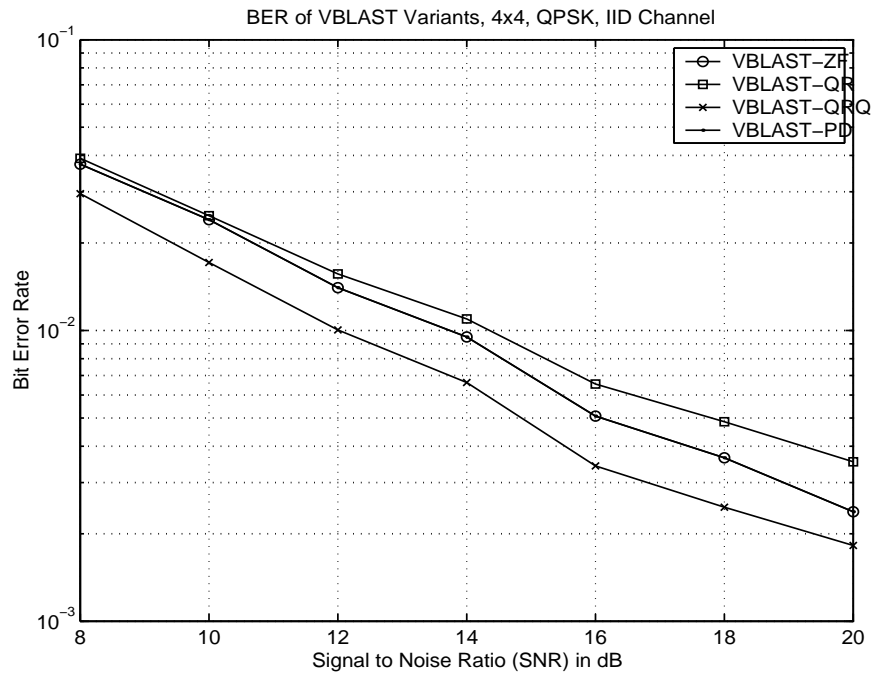


Figure 6.3: Bit error rate of different VBLAST decoding methods with optimal decoding order.

Method	Complexity
VBLAST	$8a^4 + \frac{83}{6}a^3 + \frac{13}{2}a^2$
QR	$\frac{8}{3}a^3 + a^2$
QR+QL	$\frac{16}{3}a^3 + 2a^2$
Polar	$10a^3 + 2a^2$

Table 6.2: Complexities of different VBLAST methods.

**exactly the same** BER. This reinforces the claim of possible mathematical equivalence. Again, the QR method performs similar to the VBLAST method especially at lower SNR. The QR and QL method again has significantly better performance than the VBLAST method.

### 6.3.2 Execution Time

Developed in past chapters, Table 6.2 shows the computational costs of the decoding methods for the VBLAST architecture. These numbers are just worst case operation counts, and the actual operation counts depend on many factors- yet they represent

the relative complexity. A plot of these complexities is shown in Fig. 6.4. In this study, the actual operation counts are not reported as there is no reliable known way (in MATLAB or in any tool ) to count the number of operations. So the time they take is compared to show the merit of the decoding methods. The time required by a method is called the execution time. A plot of the execution times is shown in Fig. 6.5. However, it is assumed that each execution time has two components: the CPU time (the time required for core operations) and the memory access time plus the time required for other operations. The time required for other operations is measured by running the same simulation but turning the decoding module off. The CPU time then represents the real time spent by a decoding method and can be found by subtracting the time required for other operations from the execution time. The CPU times are shown in Fig. 6.6. This shows the comparative merit of the decoding methods. As seen from the figure, the Polar Decomposition based decoding method takes the least time. Unfortunately, even though the QR+QL method achieves good throughput performance, it also takes the maximum amount of time.

## **6.4 VBLAST System vs SVD-based System**

In this set of simulations VBLAST and SVD-based MIMO systems are compared. These two MIMO architectures have different modes of operation and therefore perform differently under different channel conditions. So, to see the behavior and performance of both systems, the following channel models are used: an IID random channel, a rank deficient IID channel, a slow fading channel and a measured channel .

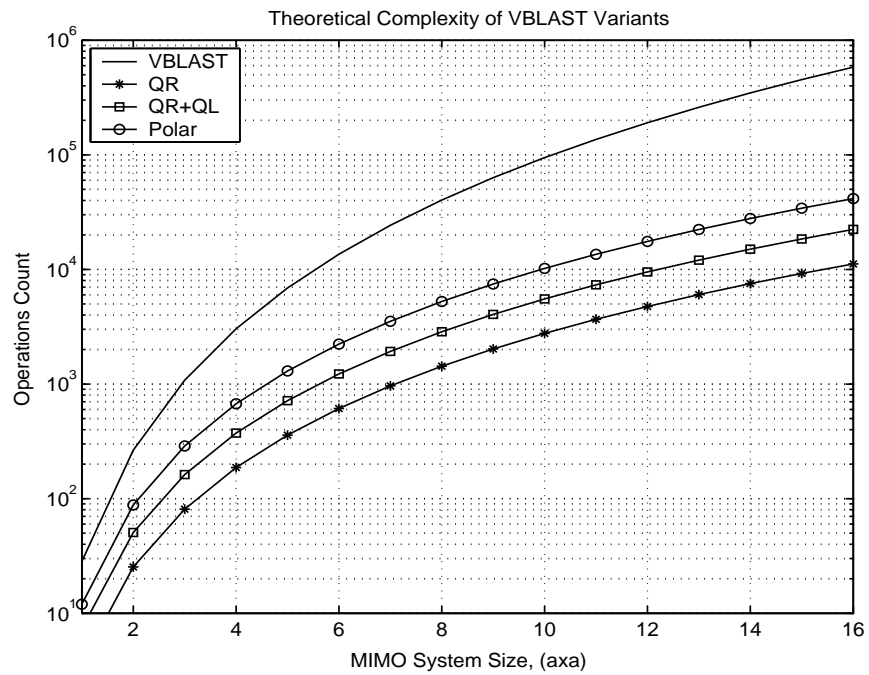


Figure 6.4: Theoretical complexity of VBLAST decoding methods.

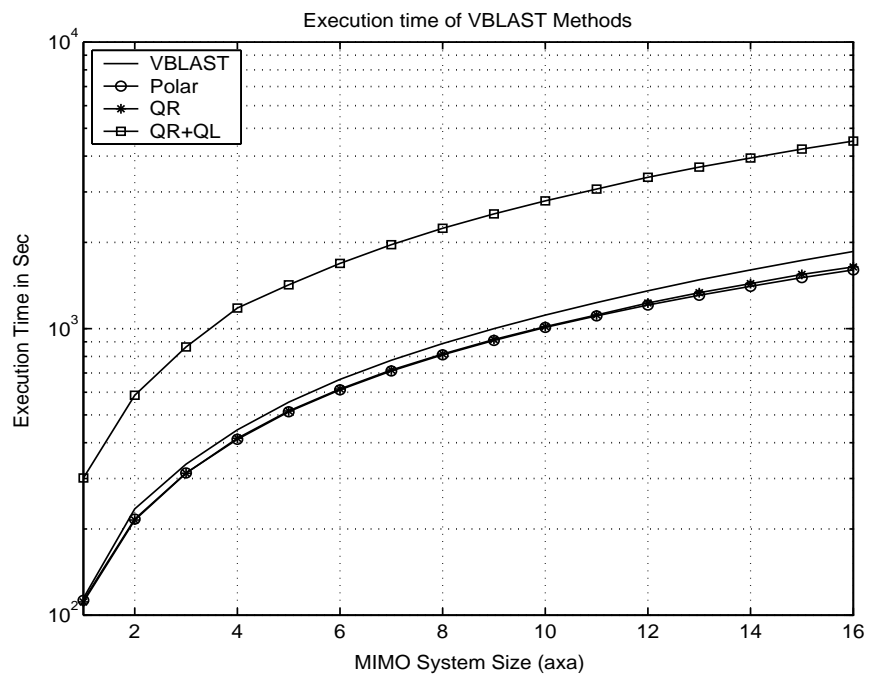


Figure 6.5: Execution time of VBLAST decoding methods.

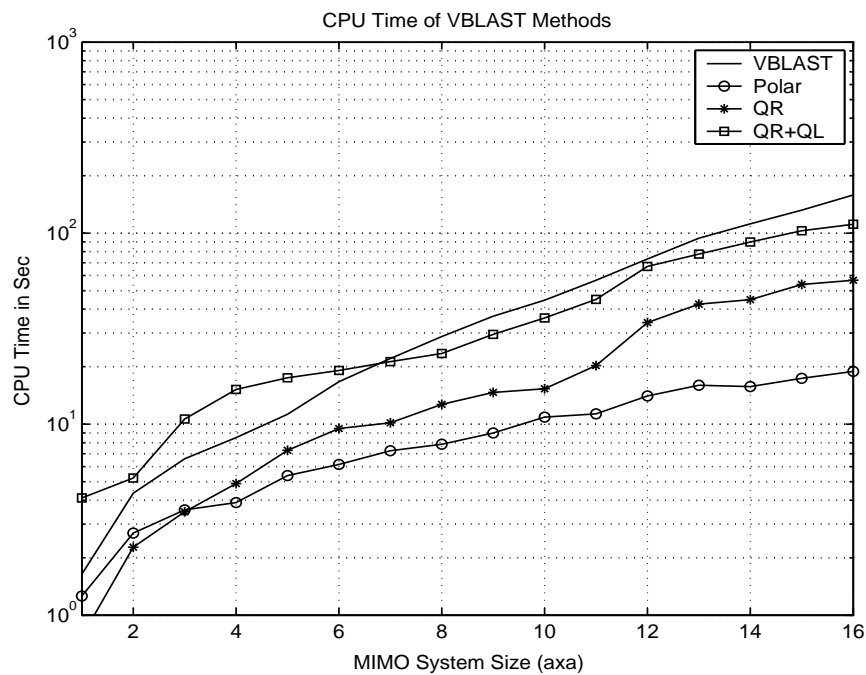


Figure 6.6: CPU time of VBLAST decoding methods.

### 6.4.1 IID Channels

The VBLAST system uses a fixed QPSK constellation because a larger constellation means a higher BLER and so a lower throughput (as reported in chapter 3). The simulation results are shown in Fig. 6.7. The top line is the average theoretical capacity that can be obtained from a  $4 \times 4$  MIMO system. As the SNR increases, VBLAST's throughput settles at 8bps/Hz, the maximum for a  $4 \times 4$  QPSK system. Though the MMSE criterion attains a slightly higher throughput, it is still far below the theoretical capacity. The SVD system with fixed QPSK performs even worse. The reason is that the weaker subchannels are too weak to accommodate even QPSK. Whereas the adaptive SVD performs the best with increasing SNR. This increase also follows the theoretical capacity, closely maintaining an almost constant gap of about 6dB. Such a 6dB gap for an uncoded system has also been reported in [10] and other

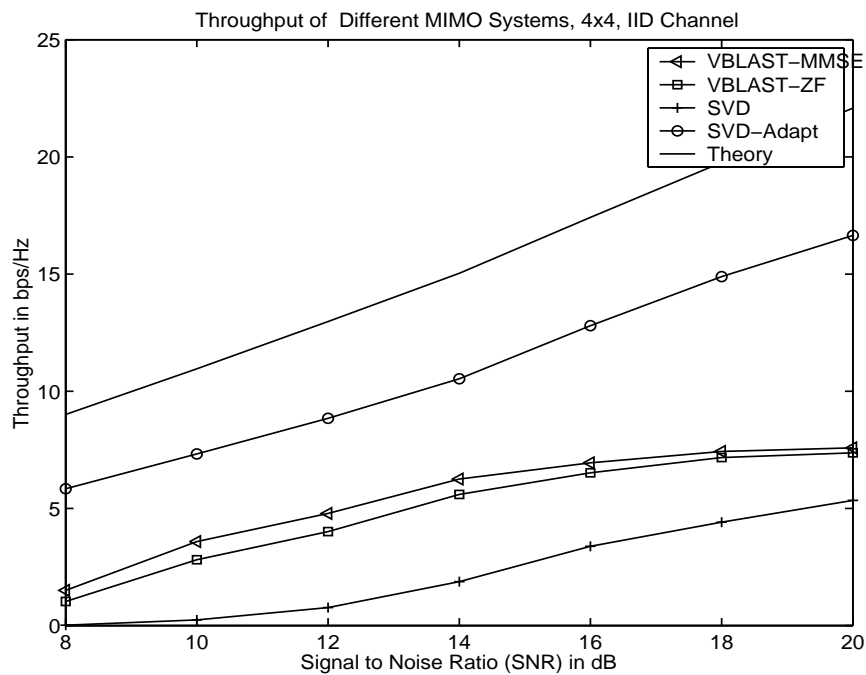


Figure 6.7: Throughput of different MIMO systems.

papers.

The throughput values are directly related to the BLER of the systems and are shown in Fig. 6.8. As expected, the BLER for a fixed SVD system is much higher than the others. The SVD-adapt system should have a flat curve for ideal adaptation. The BERs computed end to end are shown in Fig. 6.9. One noticeable thing here is that the SVD system has a slightly higher BER than the VBLAST-ZF, yet its BLER is much higher. Again, this is due to the fact that most of the block errors in the SVD system are caused by the weaker subchannels, and even a single bit error is considered to cause a block error. The zigzagness of the SVD-adapt system is caused by the discrete adaptation of the signal constellation sizes.

Using the optimal decoding order, the performance of the VBLAST system

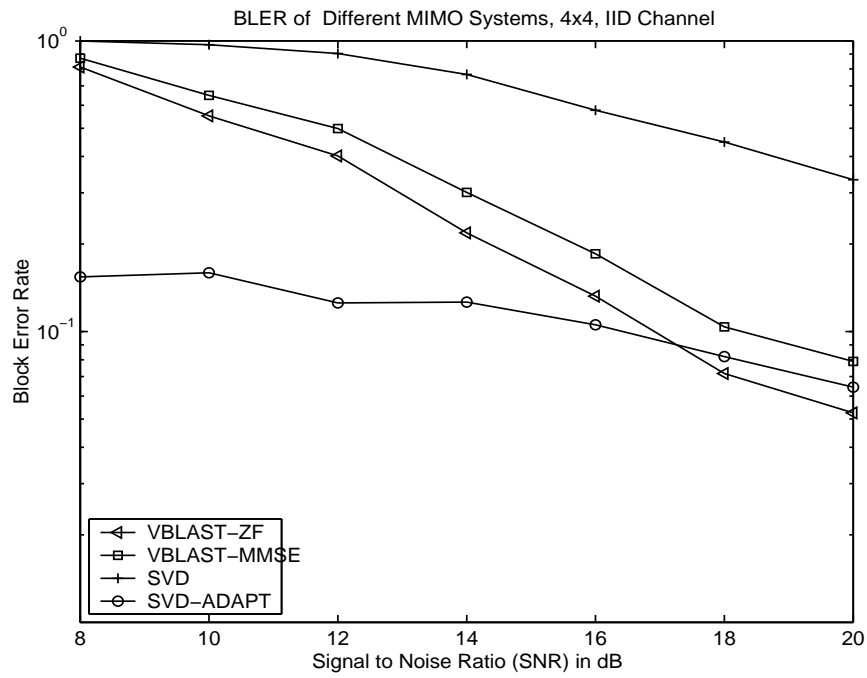


Figure 6.8: Block error rate of different MIMO systems.

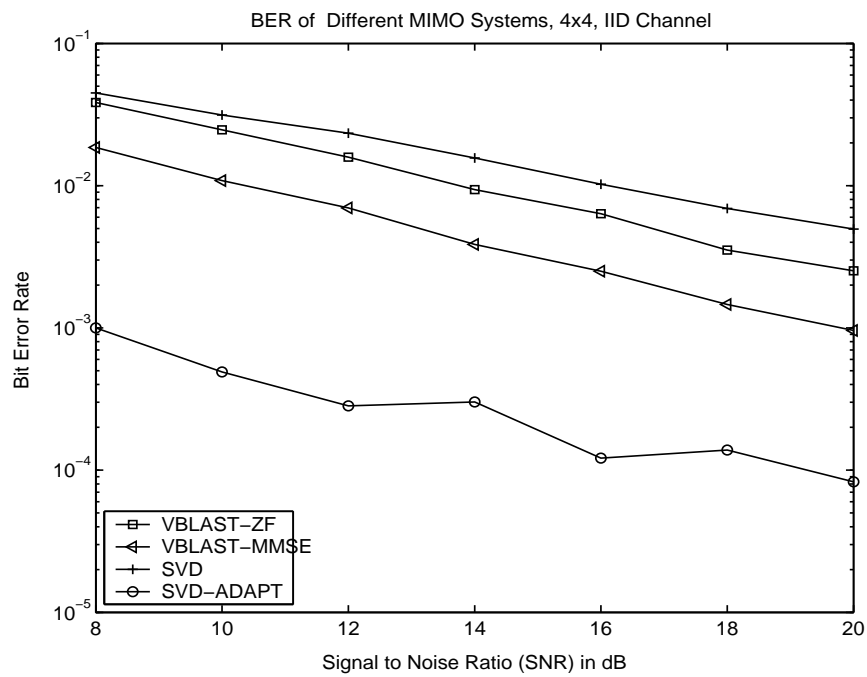


Figure 6.9: Bit error rate of different MIMO systems.

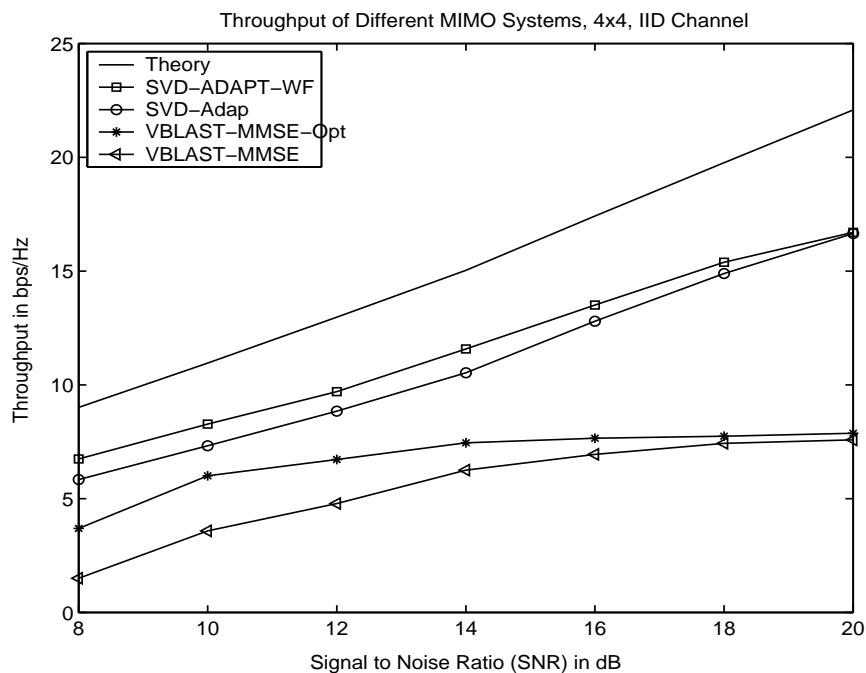


Figure 6.10: Effect of the optimal order and waterfilling.

improves slightly at the expense of some extra computational cost, whereas, the SVD-adapt system can use power control to improve its performance. The VBLAST system uses only equal power. Fig. 6.10 shows the throughput under such conditions. As seen, waterfilling is of little help and only at very low SNRs. On the other hand, optimal ordering can also help improve the throughput.

So, the SVD-based system clearly outperforms the VBLAST system in terms of throughput. This is under the assumptions that the channel is IID, the transmitter (and of course the receiver) knows the channel perfectly, and the receivers have perfect estimates of the SNR.

## 6.4.2 IID Rank Deficient Channel

The IID rank deficient channels are the same as the IID channels except the rank of the channel matrix is altered synthetically. This synthetic process involves computing

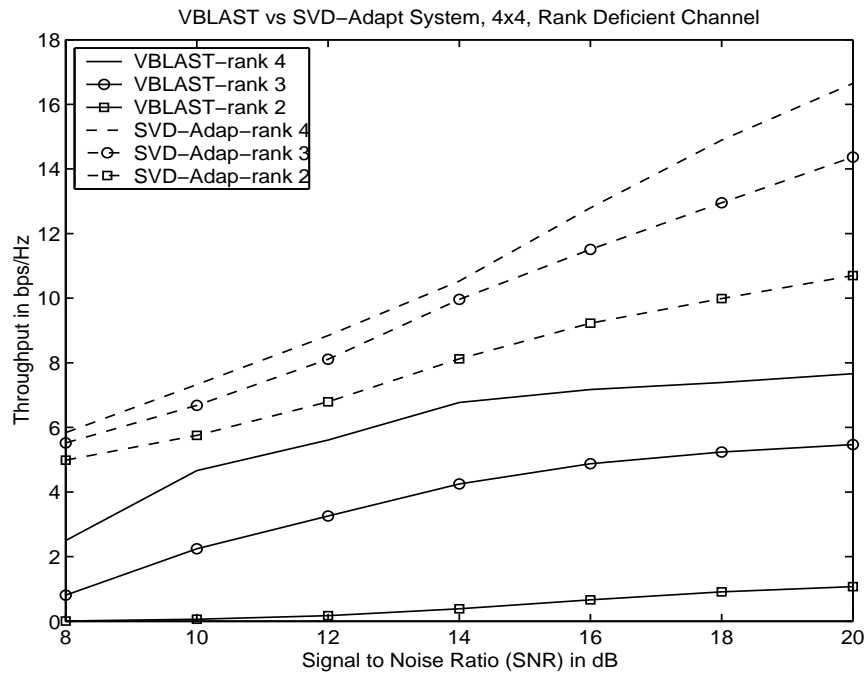


Figure 6.11: Throughputs of VBLAST-ZF-opt and SVD-adap systems in rank deficient IID channel.

the SVD ( $U, D, V$ ) of the channel matrix, setting the small unwanted singular values in  $D$  to zero and forming the new channel matrix from the product of  $U$ , the new  $D$  and  $V$ .

Fig. 6.11 shows the throughput of VBLAST and SVD systems in rank deficient IID channels. The rank is varied from 4 (full rank) to 1. The VBLAST throughput declines with decreasing channel rank whereas the SVD system can cope with the changing channel rank thanks to the adaptive modulation. The BER curves shown in Fig. 6.12 demonstrates why the VBLAST throughput drops off.

### 6.4.3 Slow Fading Rayleigh Channel

The throughput performances of the VBLAST and SVD-adapt systems are shown in Figs. 6.13 and 6.14. During simulations  $F_d T$  values of 0.002, 0.01 and 0.05 seconds

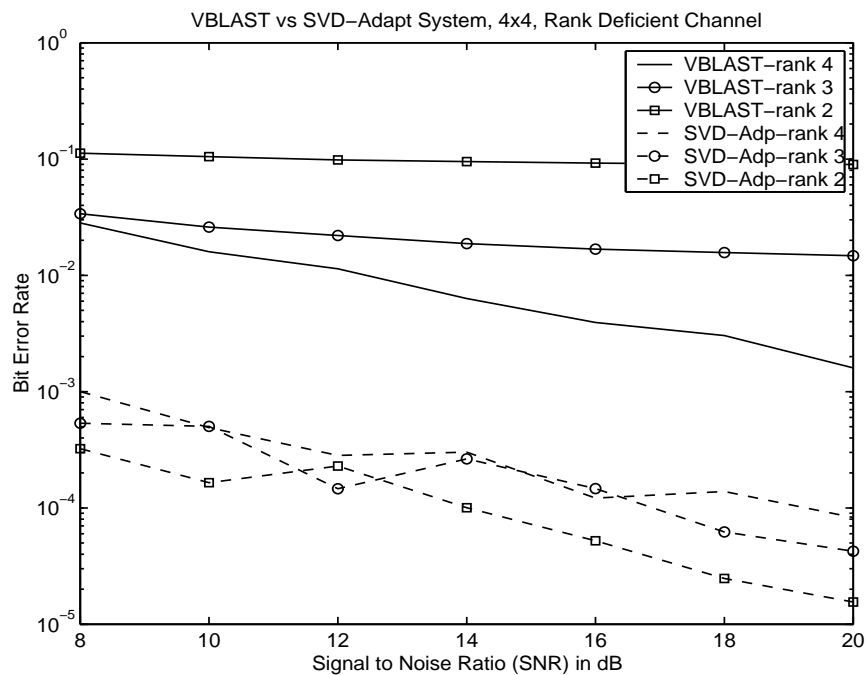


Figure 6.12: Bit error rate of VBLAST-ZF-opt and SVD-adapt systems in rank deficient IID channel

were used. Looking at any of the graphs, it is evident that the incorrect channel information has an adverse effect on both of the systems. However, the SVD-adapt system seems to be more affected than the VBLAST system. The reason for this is the sharp change in the  $U, V$  matrices for even a slowly changing channel matrix. The SVD system designers have to consider this problem seriously.

#### 6.4.4 VUT Measured Channel

The characteristics of the measured MIMO channel can be best observed by looking at the singular values of the channel samples. Before doing this, the measured data are normalized so that they are zero mean and unity variance. Fig. 6.15 shows the singular values of the measured channel samples at the LOS location. The singular values of the channel samples at the NLOS point are shown in Fig. 6.16.

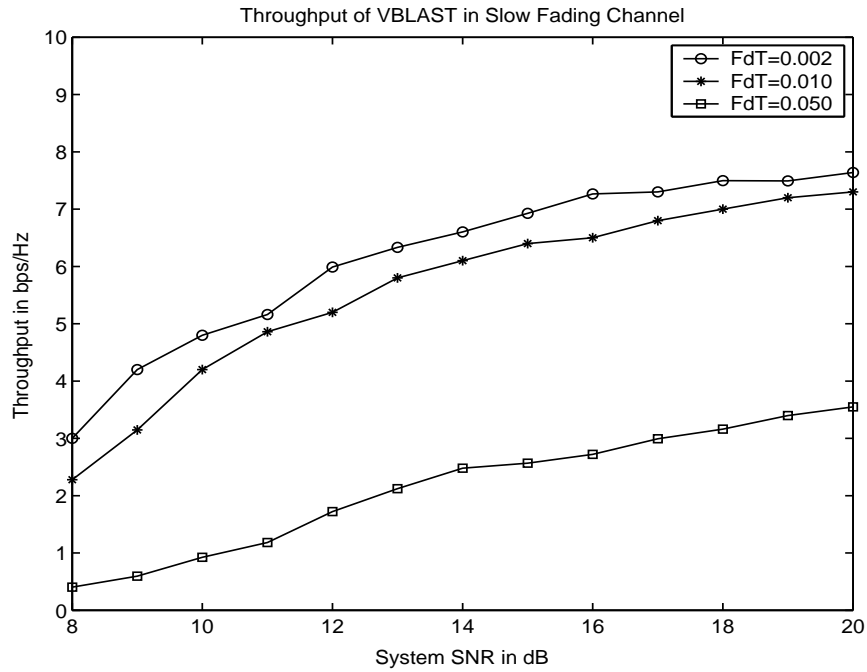


Figure 6.13: Throughput of VBLAST-opt system in slow fading Rayleigh channel.

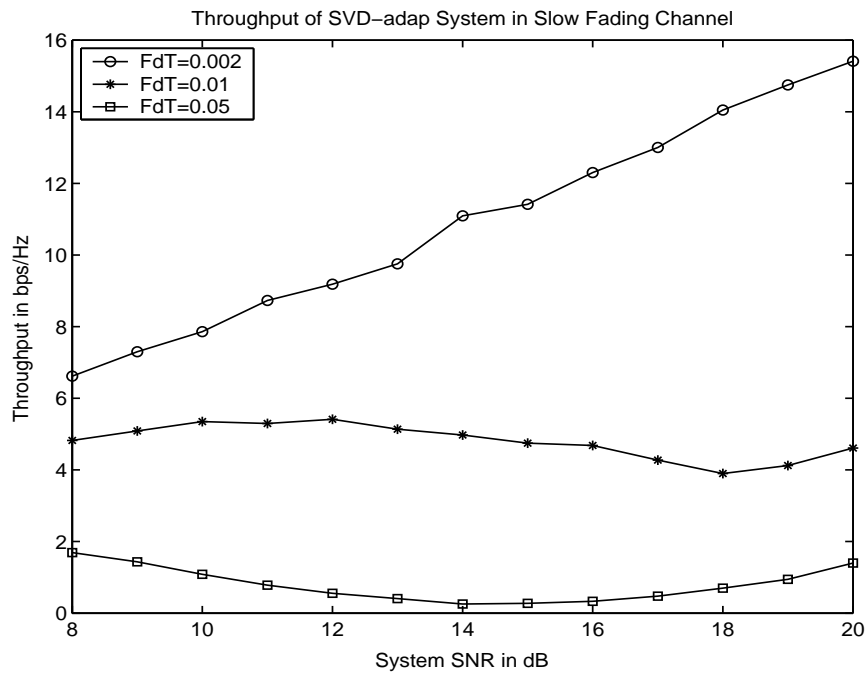


Figure 6.14: Throughput of SVD-adapt system in slow fading Rayleigh channel.

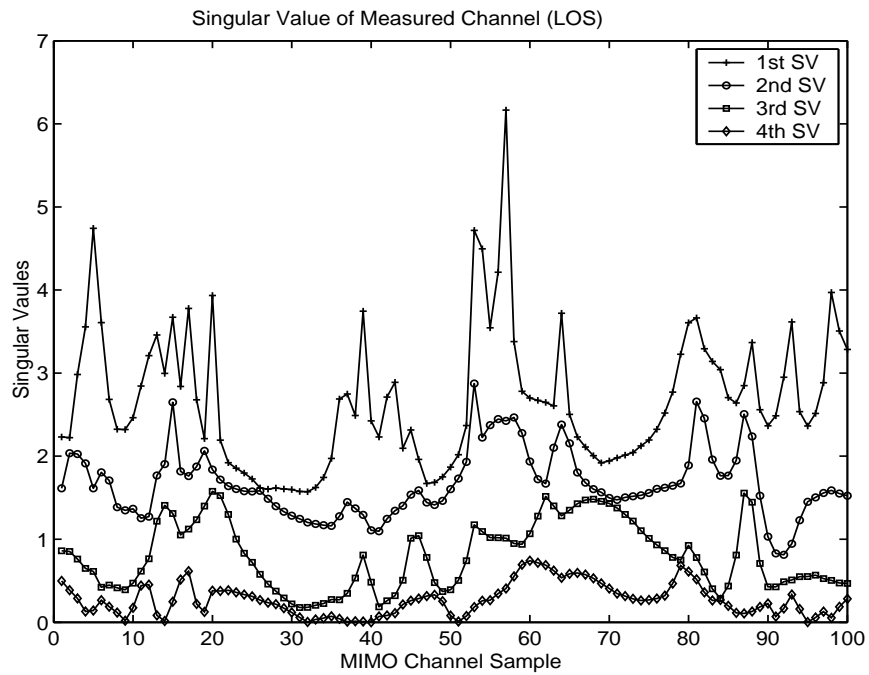


Figure 6.15: Singular values of measured channel with LOS path.

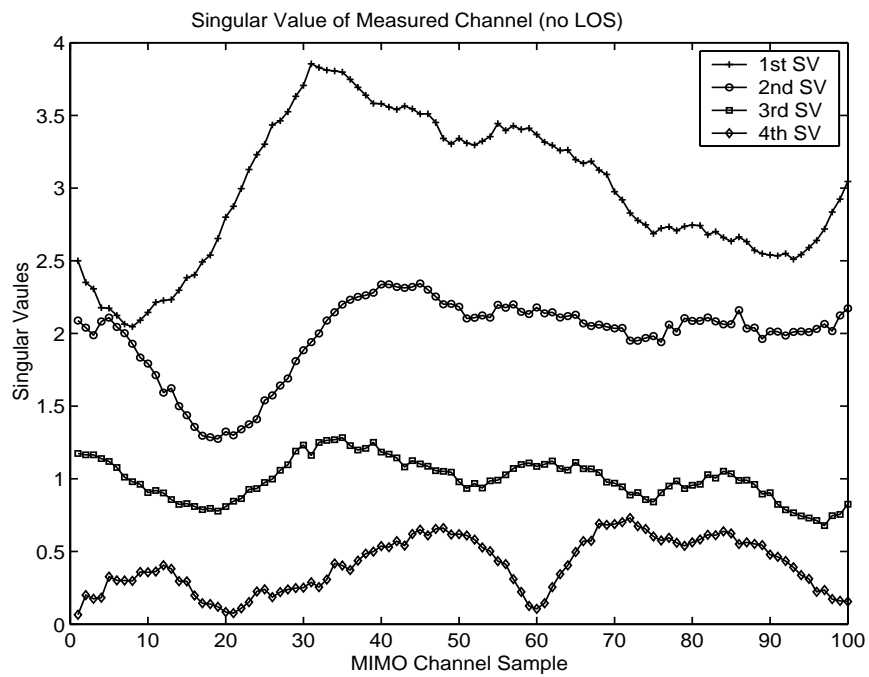


Figure 6.16: Singular values of measured channel with NLOS path.

As seen in Fig. 6.15, the presence of a LOS path does not necessarily mean that there cannot be other useful propagation paths. In a  $4 \times 4$  MIMO system, there can be at best four subchannels, the gains of which are the square roots of the singular values. Though four subchannels are shown in Fig. 6.15, the gains of the 3rd and 4th subchannels are much weaker than the first two. This means that in this LOS path environment at best two subchannels are useful and using MIMO systems with higher dimensions is of little use. In contrast, in the NLOS path environment, (Fig. 6.16) all the subchannels have comparable gains. In addition to this fact, the subchannels in the LOS case are more correlated than those in the NLOS case. Table 6.3 shows the correlation among the singular values in both cases.

However, it should be noted that the subchannels for the LOS case are much stronger than those for the NLOS case. The results for the LOS case are normalized to make a fair comparison with the NLOS case; in reality, the two 'good' subchannels of the LOS case can transmit much more data.

	LOS				No LOS			
	Sv1	Sv2	Sv3	Sv4	Sv1	Sv2	Sv3	Sv4
Sv1	1.0000	0.4296	0.2369	0.1081	1.0000	0.2344	0.1521	0.0225
Sv2	0.4296	1.0000	0.5340	0.2138	0.2344	1.0000	0.2486	0.1525
Sv3	0.2369	0.5340	1.0000	0.3374	0.1521	0.2486	1.0000	0.3078
Sv4	0.1081	0.2138	0.3374	1.0000	0.0225	0.1525	0.3078	1.0000

Table 6.3: Correlation among the singular values of measured channels.

The throughput values of the VBLAST and SVD-adapt systems are shown in Fig. 6.17. The behavior is similar to those for the IID channel. The BER values are reported in Fig. 6.18. Once again the curves are similar to those for the IID channel.

Thus, the SVD-based MIMO system performs better for all of the channel

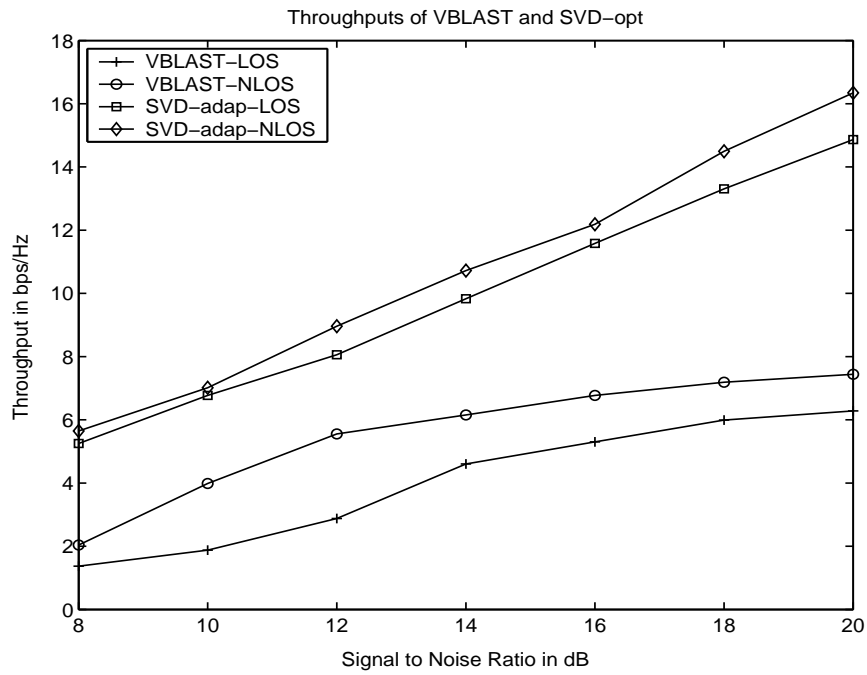


Figure 6.17: Throughputs of VBLAST-ZF-opt and SVD-adapt systems in measured channel.

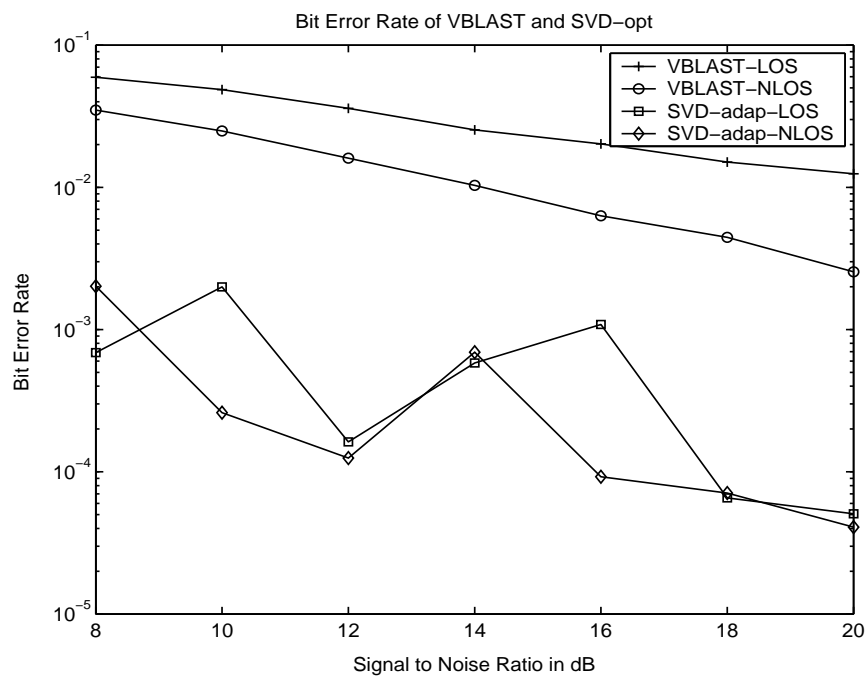


Figure 6.18: Bit error rates of VBLAST-ZF-opt and SVD-adapt systems in measured channel.

conditions. Moreover, it can adapt to the changing conditions of rank of the channel. However, in a slow fading channel, the SVD system is more sensitive to the changes in the channel, and incorrect channel information can severely affect the performances.

# Chapter 7

## Conclusion and Further Work

This thesis compares two MIMO architectures, namely VBLAST and SVD, in terms of performance and computational time. Furthermore, novel decoding algorithms for the VBLAST system have been studied and compared. In addition, a new decoding algorithm has been proposed which has the same BER performance as the original VBLAST system but takes less time for execution. Comparing the VBLAST and SVD systems, it is concluded that the SVD system achieves a capacity close to the theoretical limit. In rank deficient channels, the VBLAST system fails unless modified, whereas the SVD system can perform properly without any difficulty. However, for time varying channels accurate channel information is critical for the operation of the SVD system. With inaccurate channel information, the SVD system can collapse. As a result, SVD systems are more suitable for TDD channels where the traffic is symmetrical in both directions. For asymmetric traffic the SVD system has a huge overhead and in that case the VBLAST system would be better. So the conclusion is that both of the systems have advantages in different environments for different applications.

The new VBLAST decoding algorithm proposed here uses the Polar Decomposition of the channel matrix. In this study an existing algorithm has been used for computing the Polar Decomposition. No effort has been made to optimize the algorithm. This is an area where this work can be extended. Fixed-point implementation of this decoding method is also to be done. As it has been shown, the Polar Decomposed matrices do not change fast, and there is a real possibility of devising an incremental algorithm for the slowly varying channel matrix. In this case the Polar Decomposition need not to be calculated for every snapshot of time. Rather, results from the previous calculation may be used.

# Bibliography

- [1] C. E. Shannon, "A Mathematical Theory of Communication," *Bell Sys. Tech. Journal*, vol. 27, pp. 379-423, 1948.
- [2] W. Jakes Jr., "Microwave Mobile Communications," *John Wiley & Sons*, New York, 1974.
- [3] W. C Lee, "Effects on Correlation Between Two Mobile Radio Base Station Antennas," *IEEE Trans. on Communications*, vol. com-21, no. 11, pp. 1214-1224, November 1974.
- [4] C. E. Proakis, "Digital Communications," *McGraw-Hill International Editions*, New York, 4th edition, 2000.
- [5] A. J. Goldsmith and S. G. Chua, "Variable Rate Variable Power MQAM for Fading Channels," *IEEE Trans. on Comm.*, vol. 45, no. 11, pp. 1218-1230, October 1997.
- [6] D. Applebaum, "Probability and Information - An Integrated Approach," *Cambridge University Press*, Cambridge, UK, Chapter 6, 1996.
- [7] E. Telatar, "Capacity of Multi-antenna Gaussian Channels," *Technical Memorandum*, AT&T Bell Laboratories, 1995.

- [8] P. J. Smith and M. Shafi, "Waterfilling methods for MIMO systems," in *Proc. of the 3rd AusCTW*, Australian National University, February 2002.
- [9] C. Chua, D. Tse, J. Kahn and R. Valenzuela, "Capacity Scaling in MIMO Wireless Systems under Correlated Fading," to appear in *IEEE Trans. on Info. Theory*.
- [10] S. Catreux, P. F. Driessen and L. J. Greenstein, "Attainable Throughput of an Interference-Limited MIMO Systems," *IEEE Trans. on Comm.*, vol. 49, no. 8, August 2002.
- [11] G. J. Foschini and M. J. Gans, "On Limits of Wireless Communications in a Fading Environment when Using Multiple Antennas," *Wireless Communications Magazine*, vol. 6, pp. 311-335, 1998.
- [12] G. D. Golden, G. J. Foschini, R. A. Valenzuela and P. W. Wolniansky, "Detection Algorithm and Initial Results using VBLAST Space-Time Communication Architecture," *IEE Electronics Letters*, vol. 35, no. 1, Jan. 1999.
- [13] P. W. Wolniansky, G. J. Foschini, G. D. Golden and R. A. Valenzuela, "VBLAST: An Architecture for Realizing Very High Data Rates Over the Rich-Scattering Wireless Channel," *Bell Labs, Lucent Tech.*, available online at <http://mars.bel-labs.com>
- [14] Stephen Baro, Gerhard Bauch, Aneta Pavlic and Andreas Semmler, "Improving BLAST Performance Using Space Time Block Codes and Turbo Decoding," *Institute for Communications Engineering, Munich University of Tech*, available online at NEC ResearchIndex (<http://citeseer.nj.nec.com/cs>).

- [15] M. O. Damen, K. A. Meraim and S. Burykh, "Iterative QR Detection for BLAST," *In the Proc. of 38th Allerton Conference of Communications*, Illinois, Oct. 2000.
- [16] G. H. Golub and C. F. Van Loan, "Matrix Computations," *Johns Hopkins University Press*, 3rd edition, Baltimore, MD, 1996.
- [17] N. J. Higham, "Computing the Polar Decomposition-with Applications," *SIAM J. Sci. Stat. Computing*, vol. 7, no. 4, pp. 1160-1174, October 1986.
- [18] N. J. Higham and R. S. Schreiber, "Fast Polar Decomposition of an Arbitrary Matrix," *SIAM J. Sci. Stat. Computing*, vol. 11, no. 4, pp. 648-655, July 1990.
- [19] W. Gander, "Algorithms for the Polar Decomposition," *SIAM J. Sci. Stat. Computing*, vol. 11, no. 6, pp. 1102-1115, November 1990.
- [20] A. A. Dubrulle, "An Optimum Iteration for the Matrix Polar Decomposition," *Electronic Transaction on Numerical Computing*, Kent State University, vol. 8, pp. 21-25, 1999.
- [21] G. Lebrun, T. Ying and M. Faulkner, "MIMO Transmission over a Time Varying TDD Channel Using SVD," *IEE Electronics Letters*, vol. 37, no. 22, pp. 1363-1364, 2001.
- [22] G. Lebrun, J. Gao and M. Faulkner, "MIMO Transmission over a Time Varying TDD Channel Using SVD," *In the Proceedings of IEEE Globecom 2002*.
- [23] T. S. Rappaport, "Wireless Communications - Principles and Practice," *Prentice Hall*, Upper Saddle River, New Jersey, 1996.

- [24] Personal contact with Professor Mike Faulkner, Victoria University of Technology, Melbourne, Australia.
- [25] M. Faulkner, T. Ying, M. Mewburn and M. Pereira, "MIMO Measurement Database", Internal Technical Document, VUT, Melbourne, Australia.
- [26] G. Lebrun and M. Faulkner, "Analysis of Singular Value Decomposition Applied to Wireless Communications," *In the Proceedings of 2nd ATCRC Telecom and Networking Conference and Workshop*, October 2002, Perth, Australia.

# Publications

- Alamgir Mohammed, "On the Performance of different MIMO systems using Adaptive modulation" *In Proc of 2nd ATcrc Telecom and Networking Conference and Workshop*, 16-18 October, 2002, Freemantle, Perth, Australia.